Investigation of Trimethoprim Removal Using LED-UV/Chlorine Process

Fei Liang

Investigation of Trimethoprim Removal Using LED-UV/Chlorine Process

By

Fei Liang

in partial fulfillment of the requirement for the degree of

Master of Science

In Civil Engineering

At **Delft University of Technology**

&

Master of Science

In Hydraulic Engineering and Water Resources Management

At **National University of Singapore**

Supervisor	Prof. dr. Jiangyong Hu	NUS
Thesis Committee	Prof. dr. ir. Jan Peter van der Hoek	TUDelft
	Prof. dr. ir. Bas Heijman	TUDelft
	Prof. dr. ir. Ruud van Ommen	TUDelft

Acknowledgement

I would like to first give my heartfelt thanks to my supervisors at NUS: Teo Ying Shen and Prof. Hu Jiangyong, for giving me the opportunity to work with them and their undivided support on graduation procedure. I would like to offer my great appreciation to my thesis committee: Prof. Jan Peter van der Hoek, Prof. Bas Heijman and Prof. Ruud van Ommen. Even though the UV/Chlorine AOP that I was working on is hardly applicable in the Netherlands' context, they acknowledged the hard work that I have put in and provided me with valuable and constructive advice so that I can understand my work deeper. Not forgetting the time differences, caused much inconvenience and effort on the committee's part to schedule a suitable time for both of us to conduct our online meeting sessions.

My gratitude also goes to Dr. Jung Youmi and Dr. Cai Qinqing for being there to guide me whenever there were experimental roadblocks. And many thanks to my friends Li Lexue and Wang Yundan, who provided me with continual encouragement and tips to make my learning a smooth sailing one. I would also like to thank my 'voice companions' during my MSc study at Delft and Singapore. Chen Luyu, whose opinions and stories always resonate with me and help me learn to accept myself. Lei Guangxia, a music poet, whose songs give me quiet strength in times of uncertainty and failures.

Most importantly, I would like to express my very great thanks to my parents, for constantly believing in me and relating to my problems and issues I faced.

Abstract

UV/chlorine, as an emerging advanced oxidation process, is able to degrade organic micropollutants in water via the generation of reactive oxidant species and direct reaction with $HOCl/OCl^-$ as well. In this study, light-emitting diodes (LEDs) were applied as the UV sources to investigate the efficacy of UV/chlorine process for the degradation of trimethoprim (TMP, a frequently detected antibiotic in waters), at slightly alkaline pH.

The degradation of TMP followed the pseudo-first-order kinetics and the fluence-based rate constant (k_f') increased as pH was increased from 6 to 9 for 265nm-, 275nm- and 310nm-LED-UV/chlorine. The highest degradation rate constant in this work was around 0.275 cm^2/mJ, which was obtained at the wavelength of 275 nm and pH 9 ($[TMP]_0$=200 μg/L, $[chlorine]_0$=3 mg/L as Cl_2). The UV wavelength at 275 nm achieved higher k_f' values than 254 nm, 265 nm and 310 nm in the pH range of 7-9. The effect of pH and wavelength on the degradation of TMP during UV/chlorine process could be explained by the photolysis of chlorine and the reactions of various radicals with TMP at different pH and wavelengths. When the chlorine dosage was increased from 0.3 mg/L to 3 mg/L, the rate constants of TMP degradation increased almost linearly with the chlorine dosage, however, this was not the case when the chlorine dosage was further increased to 6 mg/L. Additionally, the presence of humic acid in water inhibited the removal of TMP in the UV/chlorine system. The preliminary analysis of TMP degradation products implicated that the UV wavelength applied in the UV/chlorine system might affect the types of degradation products.

Overall, the results of this study verified that UV/chlorine process could be effective over wider treatment conditions other than acidic pH for the removal of TMP, and they provided some suggestions on the selection of UV wavelength and pH for the application of UV/chlorine process.

List of Figures

Figure 1-1: Illustration of sources of PPCPs in water environment 1
Figure 1-2: Chemical structure of trimethoprim..... 2
Figure 1-3: Overview and classification of different AOPs. eAOP = electrochemical AOP, cAOP = catalytic AOP, pAOP = physical AOP. The colors of the boxes represent different scales of applications. White = full-scale application, grey = investigated at lab- and pilot-scale, black = tested at lab-scale. Obtained from [29]..... 6
Figure 2-1: Electromagnetic Spectrum. Obtained from [61]..... 10
Figure 2-2: Spectral output of typical low- and medium-pressure UV lamp. Obtained from [64]. 11
Figure 2-3: Light generation mechanism of LED. Where (a) depicts initial movement of mobile carriers at p-n conjunction; (b) equilibrium; (c) light emitting when bias voltage is applied. Obtained from[57]..... 14
Figure 2-4: Chlorine and TMP speciation as a function of pH..... 17
Figure 2-5: Reported wavelength and pH effects on fluence-based rate constant of chlorine photodecomposition. 19
Figure 2-6: Measured results ($[chlorine]_0$=14.2 mg/L as Cl2, $[DOC]_0$=3.0mg C/L) from [36]. 19
Figure 2-7: Absorption spectra of HOCl and OCl^-. measured respectively at pH 5 and pH 10. Obtained from [37]..... 20
Figure 2-8: Apparent quantum yields of HOCl and OCl^- photodecay as a function of wavelength. ($[chlorine]_0$=100 μM). Obtained from [35]. 21
Figure 2-9: Structure and speciation of TMP [39] 21
Figure 2-10: UV absorption spectrum of TMP as a function of UV wavelength in aqueous phase. Obtained from [40]..... 22
Figure 3-1: Schematic diagram of experimental set-ups. (a) UV quasi-collimated beam system (254 nm); (b) UV-LED system (265/275/310 nm)..... 25
Figure 3-2: LED chip array 26
Figure 4-1: Comparison of TMP degradation by LP-UV alone, dark chlorination and LP-UV/chlorine process. Condition: UV intensity: 0.2467 mW/cm^2, $[TMP]_0$=200 μg/L, $[chlorine]_0$= 3 mg/L as Cl_2..... 29
Figure 4-2: Direct UV photolysis of TMP with different wavelengths. Condition: $[TMP]_0$=200μg/L, pH 8..... 30
Figure 4-3: TMP degradation by UV/chlorine process with various wavelengths. Condition: $[TMP]_0$=200 μg/L, $[chlorine]_0$= 3 mg/L as Cl_2, pH 8..... 31

Figure 4-4: TMP degradation by dark chlorination at various pHs. Condition: $[TMP]_0$=200 µg/L, $[chlorine]_0$= 3 mg/L as Cl_2. 33
Figure 4-5: TMP degradation by UV/chlorine process as a function of UV fluence at various pHs and wavelengths. Condition: $[TMP]_0$=200 µg/L, $[chlorine]_0$= 3 mg/L as Cl_2. 35
Figure 4-6: Fluence-based pseudo-first-order rate constants of TMP degradation by UV/chlorine at various pHs and wavelengths. Condition: $[TMP]_0$=200 µg/L, $[chlorine]_0$= 3 mg/L as Cl_2. 35
Figure 4-7: TMP degradation by 275 nm-UV/chlorine process with various chlorine dosage. Condition: $[TMP]_0$=200 µg/L, pH 8. 36
Figure 4-8: Fluence-based pseudo-first-order rate constants of TMP degradation by UV/chlorine with various chlorine dosage. Condition: $[TMP]_0$=200 µg/L, pH 8. 37
Figure 4-9: Fluence-based pseudo-first-order rate constants of TMP degradation by UV/chlorine with various concentrations of humic acid. Condition: $[TMP]_0$=200 µg/L, $[chlorine]_0$=3 mg/L as Cl_2, pH 8. 38
Figure 4-10: OBPs obtained during 275nm-LED-UV/chlorine process at 10 min 39
Figure 7-1: 254 nm LP-UV intensity measured by ferrioxalate actinometer 48
Figure 7-2: 265 nm LED-UV intensity measured by ferrioxalate actinometer 48
Figure 7-3: 275 nm LED-UV intensity measured by ferrioxalate actinometer 49
Figure 7-4: 310 nm LED-UV intensity measured by ferrioxalate actinometer 49
Figure 7-5: TMP degradation by dark chlorination at pH 6 – 9. Condition: $[TMP]_0$ = 200 µg/L, $[chlorine]_0$ =3 mg/L as Cl_2. 50
Figure 7-6: TMP degradation by LP-UV/chlorine (254 nm) at pH 6 – 9. Condition: $[TMP]_0$ = 200 µg/L, $[chlorine]_0$ =3 mg/L as Cl_2, UV intensity: 0.2467 mW/cm^2. 50
Figure 7-7: TMP degradation by 265 nm LED-UV/chlorine at pH 6 – 9. Condition: $[TMP]_0$ = 200 µg/L, $[chlorine]_0$ =3 mg/L as Cl_2, UV intensity: 0.1774 mW/cm^2. 51
Figure 7-8: TMP degradation by 275 nm LED-UV/chlorine at pH 6 – 9. Condition: $[TMP]_0$ = 200 µg/L, $[chlorine]_0$ =3 mg/L as Cl_2, UV intensity: 0.2564 mW/cm^2. 51
Figure 7-9: TMP degradation by 310 nm LED-UV/chlorine at pH 6 – 9. Condition: $[TMP]_0$ = 200 µg/L, $[chlorine]_0$ =3 mg/L as Cl_2, UV intensity: 0.1769 mW/cm^2. 52
Figure 7-10: TMP degradation by 265 nm LED -UV/chlorine process with various chlorine dosage. Condition: $[TMP]_0$=200 µg/L, UV intensity: 0.1774 mW/cm^2, pH 8. 52
Figure 7-11: TMP degradation by 310 nm LED -UV/chlorine process with various chlorine dosage. Condition: $[TMP]_0$=200 µg/L, UV intensity: 0.1769 mW/cm^2, pH 8. 53
Figure 7-12: TMP degradation by 265 nm LED-UV/chlorine with various concentrations of humic acid. Condition: $[TMP]_0$=200 µg/L, $[chlorine]_0$=3 mg/L as Cl_2, UV intensity: 0.1774 mW/cm^2, pH 8. 53

Figure 7-13: TMP degradation by 275 nm LED-UV/chlorine with various concentrations of humic acid. Condition: $[TMP]_0$=200 µg/L, $[chlorine]_0$=3 mg/L as Cl_2, UV intensity: 0.2564 mW/cm^2, pH 8. 54
Figure 7-14: TMP degradation by 310 nm LED-UV/chlorine with various concentrations of humic acid. Condition: $[TMP]_0$=200 µg/L, $[chlorine]_0$=3 mg/L as Cl_2, UV intensity: 0.1769 mW/cm^2, pH 8. 54
Figure 7-15: LC-MS/MS spectra of TMP degradation products: full scan. Condition: $[TMP]_0$ = 10 mg/L, $[chlorine]_0$ = 15 mg/L as Cl_2, UV fluence = 154 mJ/cm^2, wavelength =275 nm, pH 8. 55
Figure 7-16: LC-MS/MS spectra of TMP degradation products a) 165, b) 179, c) 183, d) 271, e) 274, f) 291(TMP), g) 307, h) 309, i) 325, j) 327, k) 341, l) 343, m) 391, n) 413, o) 445. Condition: $[TMP]_0$ = 10 mg/L, $[chlorine]_0$ = 15 mg/L as Cl_2, UV fluence = 154 mJ/cm^2, wavelength =275 nm, pH 8. 59

List of Tables

Table 1-1: Concentrations of TMP reported in wastewater treatment plants 4
Table 1-2: Concentrations of TMP reported in drinking water treatment plants..... 5
Table 2-1: Summary of major reactions in the UV/chlorine system. Adapted from [14], [30], [34]. 18
Table 2-2: Absorption coefficients and quantum yields of TMP at 254nm. Adapted from [40] 22
Table 3-1: Preparation of 0.1M Potassium phosphate buffer (1L) at 25℃ 24
Table 3-2: Parameters of UV-LEDs (T=25℃, IF=600 mA) 26
Table 3-3: Average UV intensity of the four UV systems 26
Table 4-1: TOC level of HA solution and the effect of HA on TMP degradation. Condition: same as Figure 4-9. 38
Table 4-2: Degradation products of TMP by UV/chlorine detected by LC-MS/MS ($[TMP]_0$=10mg/L, $[chlorine]_0$=15 mg/L, UV wavelength=275 nm, pH 8) 40

List of Equations

Equation 1-1 : Scavenging of • OH by H_2O_2 7
Equation 2-1: UV dose equation 11
Equation 2-2: Generation of Fe^{2+} in photochemical reaction via potassium ferrioxalate..... 12
Equation 2-3: Equation to calculate amount of Fe^{2+} generated from photochemical reaction 12
Equation 2-4: Quantum yield 13
Equation 2-5: Beer- Lambert's law 13
Equation 2-6: Quantum yield of ferrioxalate actinometer 13
Equation 2-7: Equation to calculate the amount of absorbed UV 13
Equation 2-8: Average UV intensity via application of Ferrioxalate Actinometer 14
Equation 2-9: Quantum yield of chlorine loss..... 20
Equation 2-10: Quantum yield of •OH formation..... 20
Equation 3-1: Henderson-Hasselbalch Equation..... 24
Equation 3-2: Quenching equation between $Na_2S_2O_3$ and NaClO 24
Equation 3-3: Differential equation of second-order kinetic reaction(s)..... 28
Equation 3-4: Differential equation of pseudo-first-order kinetic reaction(s)..... 28
Equation 3-5: Equation of pseudo-first-order kinetic reaction(s) expressed as a ratio of the concentration of A 28

Nomenclature

AOCl	absorbable organic chlorine
AOPs	advanced oxidation processes
CF	chloroform
CH	chloral hydrate
DAMP	2,4-diamino-5-methylprimidine
DBPs	disinfection by-products
DCAN	dichloroacetonitrile
DPD	diethyl-p-phenylene-diamine
DTP	drinking water treatment plant
HA	humic acid
HAA	haloacetic acid
HAN	haloacetonitrile
HK	haloketone
LC-MS/MS	liquid chromatography-double mass spectrometry
LED	light-emitting diode
NOM	natural organic matter
TCNM	trichloronitromethane
THM	trihalomethane
TMP	trimethoprim
TMT	3,4,5-trimethoxytoluene
OBPs	oxidation by-products
PPCPs	pharmaceuticals and personal care products
RCS	reactive chlorine species
ROS	reactive oxidant species
SMX	sulfamethoxazole
USEPA	US Environmental Protection Agency
WPE	wall plug efficiency
WWTP	wastewater treatment plant

Contents

Acknowledgement i

Abstract ii

List of Figures iii

List of Tables vi

List of Equations vii

Nomenclature viii

1 Introduction 1

1.1 Pharmaceuticals and personal care products 1

1.2 Trimethoprim in aquatic environment 2

1.2.1 Medical use of TMP and toxicity 2

1.2.2 Occurrence and removal of TMP in WWTPs and DTPs 2

1.3 Advanced Oxidation Process for TMP removal 6

1.4 UV/chlorine as an AOP for TMP removal 7

1.5 Light-emitting diodes (LEDs) as UV sources 8

1.6 Study objective 8

2 Background knowledge 10

2.1 UV radiation 10

2.1.1 Types of UV radiation 10

2.1.2 Conventional UV lamps 10

2.1.3 Determination of UV fluence 11

2.2 LED as an UV light source 14

2.2.1 Light generation mechanism of LED 14

2.2.2 Characteristics of UV-LED 15

2.2.3 Application of UVLEDs in AOPs 16

2.3 Chlorine photolysis 16

2.3.1 Radical formation 16

2.3.2 Photodecomposition rate 19

2.4 Photochemical properties of TMP 21
3 Materials and methods 23
3.1 Chemicals and solution preparation 23
3.1.1 Reagents 23
3.1.2 Solution preparation 23
3.2 UV irradiation 25
3.2.1 Experimental set-ups 25
3.2.2 UV intensity measurement 25
3.3 Experimental procedures 26
3.4 Analytical methods 27
3.4.1 Experimental analysis 27
3.4.2 Data analysis 28
4 Results and discussions 29
4.1 Degradation kinetics 29
4.1.1 TMP degradation by LP-UV alone, dark chlorination and LP-UV/chlorine 29
4.1.2 Effect of wavelength 30
4.1.3 Effect of pH 32
4.1.4 Effect of chlorine dosage 35
4.1.5 Effect of NOM (humic acid) 37
4.2 Degradation products 38
5 Conclusions and Recommendations 41
5.1 Conclusions 41
5.2 Recommendations 41
5.2.1 Experimental improvement 41
5.2.2 Further research 42
6 Bibliography 43
7 Appendix 48
7.1 Ferrioxalate Actinometry 48

7.2 TMP degradation kinetics..... 50

7.3 TMP degradation products 55

1 Introduction

1.1 Pharmaceuticals and personal care products

In recent decades, pharmaceuticals and personal care products (PPCPs) residues are frequently detected in surface and ground waters across the globe, at concentration levels of ng/L to μg/L[1]–[3]. PPCPs are known to be released into environment through several pathways (Figure 1-1), including effluent discharge from wastewater treatment plants (WWTPs), livestock breeding, fertilizing, landfill leaching and agricultural runoff, etc. Considering the increasing consumption of PPCPs, the escalating introduction of new products to the market and improper disposal, the PPCPs contamination issue in aquatic environments would be even more serious[1], [2].

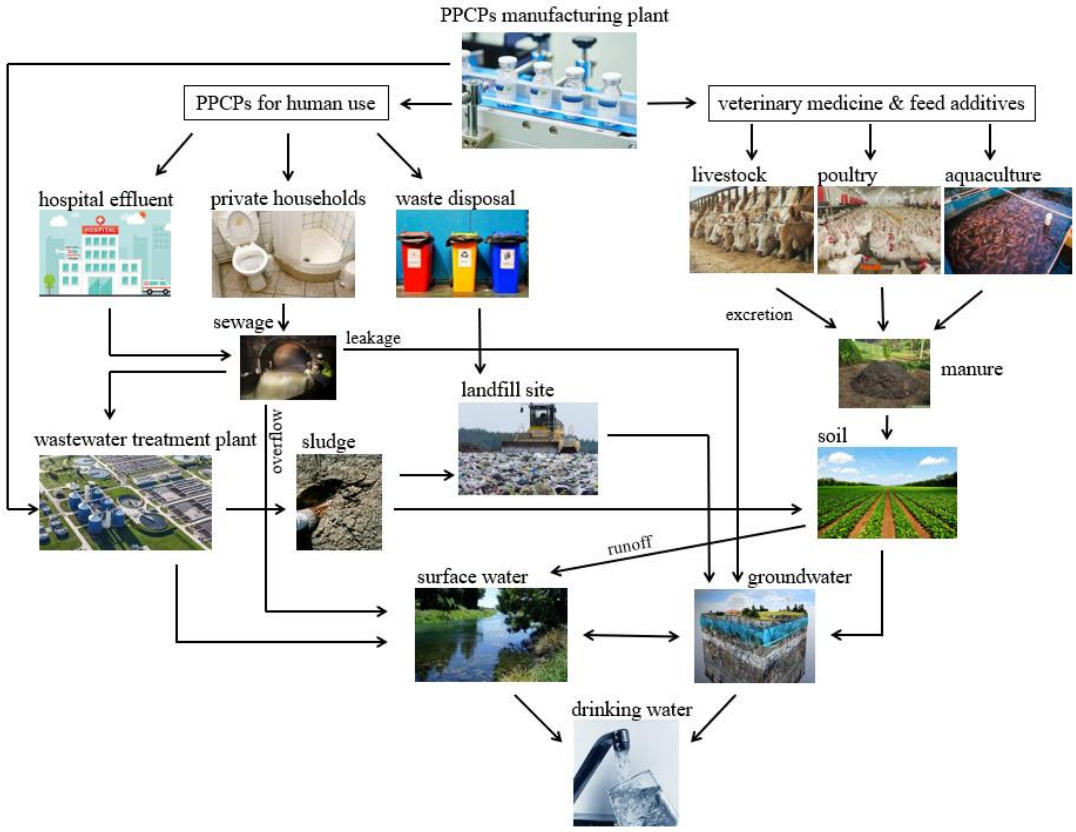

Figure 1-1: Illustration of sources of PPCPs in water environment

Currently, little is known about the direct impact of PPCPs contamination on public health. However, toxic effects of PPCPs on aquatic organisms like green algae, Daphnia magna, zebra fish and gold fish have been revealed in many studies [1], [2]. More notably, PPCPs together with their metabolites can eventually enter and accumulate in our food chain. Bioaccumulation

factors ranging from tens to tens of thousands for many pharmaceuticals were found in non-target aquatic organisms [1], [2]. Besides, even though most PPCPs detected in waters are at trace level, the toxicity arising from complex mixtures of these PPCPs may lead to synergistic interactions, and thus pose a threat to both human and environment [2], [4].

1.2 Trimethoprim in aquatic environment

1.2.1 Medical use of TMP and toxicity

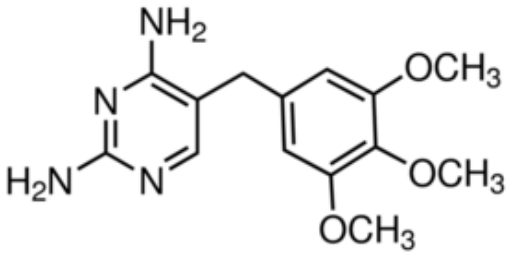

Figure 1-2: Chemical structure of trimethoprim

As an efficient and inexpensive antibiotic, Trimethoprim (TMP) has been widely used for many decades to treat bacterial infections. TMP is commonly prescribed together with sulfamethoxazole (SMX) for the treatment of urinary tract infection in humans [5]. In veterinary medicines, TMP is mainly used for therapeutic, prophylactic and growth promoting purposes [6]. After administration of TMP to humans and animals, about 46% of the applied dose is excreted through urine and feces, with 22% as unchanged TMP [7]. According to Globally Harmonized System (GHS) hazard statements, TMP residue is toxic to aquatic life with long lasting effects [8]. It is also identified as one priority substance based on the selection and prioritization mechanism for hazardous substances of the OSPAR commission [2].

1.2.2 Occurrence and removal of TMP in WWTPs and DTPs

TMP has been frequently detected in various water environments. Table 1-1 and Table 1-2 summarize the occurrence of TMP and the performance of both WWTPs and DTPs for TMP removal reported in literature. For WWTPs, the maximum concentrations of TMP were found to be 4300 ng/L and 550 ng/L in raw influent and final effluent, respectively; While in DTPs, the reported maximum TMP levels were 150 ng/L in source water and approximately 20 ng/L in finished drinking water.

Reports about the TMP removal performances in WWTPs varied significantly due to the different unit processes applied, as well as the specific operation conditions. Generally, the conventional first and secondary treatment processes are not completely capable of removing

TMP in water as most WWTPs are mainly designed to remove nutrients and easily degradable carbon compounds [9]. According to previous studies, only a minor elimination of up to 20% was achieved during primary treatment. This poor removal was explained by the low octanol-water partition coefficient of TMP ($\log K_{ow}$ = 0.791~0.91) [10], [11], thus TMP cannot be absorbed greatly either to the particles in primary clarifiers or biomass in biological reactors. The removal efficiency by secondary treatment ranged from -54% to 100%. The negative value was believed to be due to the release of TMP in feces particles during biological treatment [12]. Besides, it's also reported that the presence of TMP might cause inhibitory effects on activated sludge bacteria which further reduces the removal rate [1]. Though it has been found that the removal efficiency could be enhanced by long sludge retention time (SRT) taking advantages of the degrading capacity of nitrification organisms [11], [12], the bio-degradation of TMP is often incomplete. In Wang et al. 's report [10], TMP was even described as 'neither biodegraded nor absorbed'. As for tertiary treatment, no significant removal was observed by solely UV disinfection (~9%); whereas granular activated carbon (GAC), powdered activated carbon (PAC) followed by filtration process, and membrane filtration alone all largely improved the elimination with the removal rate of > 90%.

Compared with WWTPs, data regarding the occurrence and removal of TMP in DTPs is less well recorded. From the limited data available, conventional processes including flocculation, coagulation and sedimentation showed a moderate TMP removal of around 50% [4]. The performance of chemical oxidation such as ozonation (~28%) and chlorination (~7%) were also relatively poor in one DTP in southeast United States [4]. The reduction of TMP relied more on the advanced treatment processes like activated carbon and membrane filtration, which is consistent with the case in WWTPs.

Collectively, the conventional treatment facilities in both WWTPs and DTPs are found to be ineffective at TMP removal, due to the complex structure and high hydrophilicity of TMP [9], [10], [12], [13]. GAC and membrane filtration perform well in TMP removal, however, the high equipment cost [14] and frequent regeneration schemes [15] make these two methods less feasible. PAC is another effective option. It can be not only applied as a post-treatment after biological process, but also dosed directly into the existing biological unit [16], which is very convenient and economical. However, additional clarifier or filtration unit is required to recycle PAC and prevent PAC loss in effluent. Besides, the direct dose or recycling of PAC into the biological treatment is not practicable if the sewage sludge is used for agricultural purposes [16]. Therefore, new technologies for more efficient TMP removal in both drinking water treatment and advanced wastewater treatment targeting (in)direct potable water reuse are needed.

Table 1-1: Concentrations of TMP reported in wastewater treatment plants

Location	Raw influent		Primary effluent			Secondary effluent			Tertiary effluent			Final effluent			Overall Removal	Reference
	Med conc. (ng/L)	Max conc. (ng/L)	Med conc. (ng/L)	Max conc. (ng/L)	Removal	Med conc. (ng/L)	Max conc. (ng/L)	Removal	Med conc. (ng/L)	Max conc. (ng/L)	Removal	Detection frequency (%)	Med conc. (ng/L)	Max conc. (ng/L)		
Mexico	590	1400	-	-	-	-	-	-	-	-	-	-	180	-	~69%	[17]
Australia	430	4300	-	-	-	-	-	-	-	-	-	91%	10	250	~97%	[18]
Australia	340	930	370	480	-8%	50	70	86%	5	10	>90%	100%	5	10	98%	[19]
			(screen + grit chamber + PC)			(CAS + SC) [a,b]			(MF + RO)							
UK	263	300	-	-	-	406	414	~-54%	-	-	-	-	271	322	-3%	[20]
			(screen + PC)			(trickling filter + AS)			(UV disinfection)							
Singapore	100	~150	-	-	-	~85	~95	<50%	-	-	-	-	-	-	-	[21]
						(CAS + SC)										
			(PC)			~50	~90	-								
						(MBR)										
China	257	-	-	-	~12%	-	-	~10%	-	-	~9%	-	186	-	~27%	[10]
			(screen + PC)			(CAS + SC)			(UV disinfection)							
Switzerland	235	287	-	-	-	158	231	12-58%	-	-	>90%	-	-	-	~94%	[22]
			(screen + grit chamber + PC)			(CAS + SC)			(PAC + UF)							
Switzerland	290	440	230	340	~20%	200	400	~13%	70	310	~65%	-	70	310	~75%	[23]
			(screen + grit chamber + PC)			(CAS /FBR)			(sand filter)							
France	64	222	-	-	-	-	-	-	-	-	84-98%	-	4	6	~95%	[24]
			(screen + grit + lamellar settler)			(3-stage biofilter)			(fluidized PAC bed (pilot))							
USA	330	1300	-	-	-	-	-	50-100%	-	-	-	-	170	550	~50%	[25]
						(CAS)										
USA	-	-	610	770	-	280	530	-21-91%	21	32	95±5%	-	<10	-	>98%	[26]
			(screen + grit chamber + PC)			(CAS + SC+ filtration)			(GAC)			(Ozonation)				

Table 1-2: Concentrations of TMP reported in drinking water treatment plants

Location	Treatment process	Source water			Finished drinking water			Removal efficiency	Reference
		Detection frequency	Med (Min) conc. (ng/L)	Max conc. (ng/L)	Detection frequency	Med conc. (ng/L)	Max conc. (ng/L)		
USA	①+②+③	100%	5.8	10.9±0.8	88%	1.5	19.8±4.5	53.8±30.1%	[4]
	①pre-ozonation + flocculation + sedimentation							43.4±22.8%	
	②intermediate ozonation							27.6±21.2%	
	③filtration + chlorination							7.4±5.7%	
Spain	①+②(or + ③)	-	(9.5)	22.8	-	-	-	99±0.2% (or >99%)	[13]
	① dioxychlorination + coagulation + flocculation + settling + sand filtration							~45%	
	② ozonation + GAC filtration							-	
	③ ultrafiltration + UV + reverse osmosis							-	
Canada	-	10%	9.6	25	-	-	15	-	[27]
Australia	-	64%	3	150	Not Detected	Not Detected	Not Detected	-	[18]

(continued from Table 1-1)
a. Technologies applied in each treatment stage.
b. PC = primary clarifier; SC = secondary clarifier; CAS = conventional activated sludge; FBR = fixed bed reactor; MBR = membrane bioreactor; PAC = powdered activated carbon; GAC = granular activated carbon; RO = reverse osmosis; MF = microfiltration; UF = ultrafiltration.
c. The removal efficiencies are either directly stated in the cited literature or calculated from the median influent and effluent concentrations.
d. - = no data

1.3 Advanced Oxidation Process for TMP removal

An example of a technology that provides efficient TMP removal is the advanced oxidation processes (AOPs). AOPs are treatment technologies designed to degrade and mineralize recalcitrant organic matter from wastewater and drinking water via the production and reactions with reactive species, mainly hydroxyl radicals (•OH) [28]. Figure 1-3 [29] gives a broad overview and classification of different technologies studied for use as AOPs.

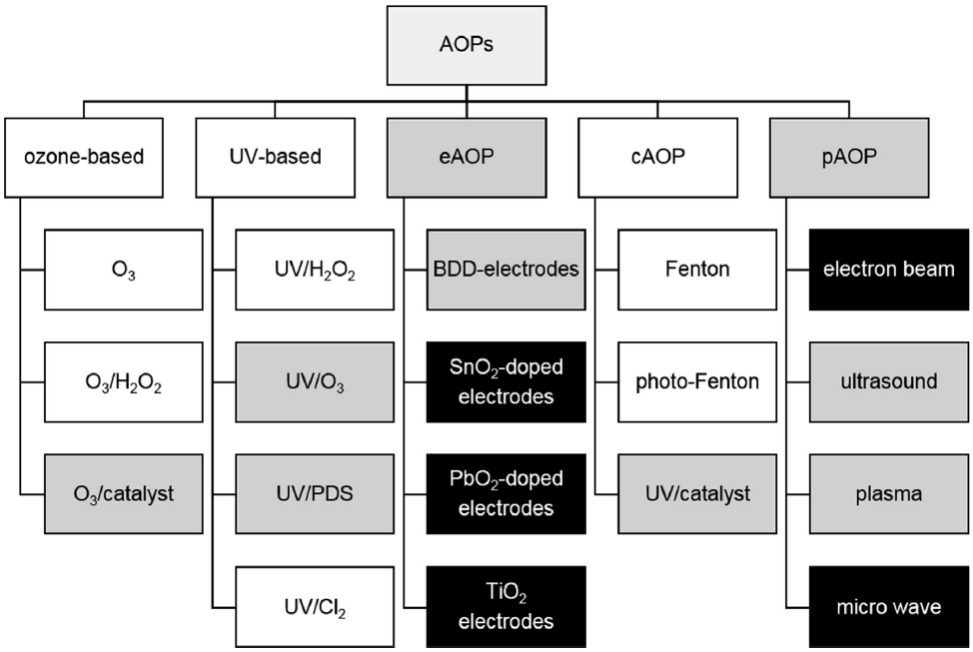

Figure 1-3: Overview and classification of different AOPs. eAOP = electrochemical AOP, cAOP = catalytic AOP, pAOP = physical AOP. The colors of the boxes represent different scales of applications. White = full-scale application, grey = investigated at lab- and pilot-scale, black = tested at lab-scale. Obtained from [29].

Among these technologies, UV/H_2O_2 is one of the most investigated and feasible options for TMP removal [5]. It possesses the following advantages:

- No significant formation of oxidation by-products (OBPs) [30];
- Lower cost than O_3-based AOPs [31];
- Consistent performance over a wide UV wavelength range [32].

Unfortunately, the application of this process is limited by the relatively low UV absorbance of H_2O_2 ($\varepsilon_{254,\ H2O2}$ = 19.6 $M^{-1}cm^{-1}$) [33]. Moreover, the •OH produced can be depleted by H_2O_2 (if it is in excess concentrations). This is known as the scavenging effect [33], [34]. Generally, 75-90% of the influent H_2O_2 remains unphotolyzed after the treatment process, thus higher costs arise due to the necessity of quenching residual H_2O_2 and the need to build an extra treatment

process to accommodate the quenching [32], [35]. In the Andijk DTP of the Netherlands, UV/H_2O_2 is applied for disinfection and organic pollutant control, and the excess H_2O_2 is quenched by GAC filtration [30], [36].

$$\bullet OH + H_2O_2 \xrightarrow{k_{H_2O_2}} HO_2 \bullet + H_2O \qquad k_{H_2O_2} = 2.7 \times 10^7\ M^{-1}s^{-1}$$

Equation 1-1 : Scavenging of • OH by H_2O_2

1.4 UV/chlorine as an AOP for TMP removal

The UV/chlorine process, is a rising alternative to the UV/H_2O_2 process and has attracted growing interest. It is able to:

- Utilize existing infrastructure without introducing major process flow modifications to the plant [37], [38];
- Remove target pollutants by multiple oxidative pathways and mechanisms [37]–[46]
    a. Oxidation by reactive species;
    b. direct reaction with HOCl/OCl^-;
    c. direct photolysis by UV radiation.
- Be more efficient than the conventional UV/H_2O_2 process due to the higher molar absorption coefficients ($\varepsilon_{254,\ HOCl(OCl^-)}$ = 59 (66) $M^{-1}cm^{-1}$), which results in lower chemical and energy costs [32], [33], [39], [41].

In Wu et al.'s study, the degradation of TMP was faster by UV/chlorine process than UV/H_2O_2 at pH 7.1 and the same oxidant concentrations, which may due to the contribution of reactive chlorine species (RCS) including ClO•, Cl• and $Cl_2^{-\bullet}$ in UV/chlorine system [5]. Similar findings were also observed for the degradation of other pharmaceuticals such as ibuprofen, carbamazepine, sulfamethoxazole and diclofenac [47]–[49]. UV/chlorine has already been put into full-scale application for indirect potable water reuse in Los Angeles [50].

However, free chlorine as well as other chlorine species can react with dissolved organic matter to form OBPs including trihalomethane (THM) and haloacetic acid (HAA) groups, which are carcinogenic to human and animals when present in sufficient quantities [34]. This risk of OBPs (or DBPs) coupled with consumers' dislike of the taste and odor of residual chlorine caused some European countries, including the Netherlands, Germany, and Switzerland, to move toward a chlorine-free treatment [51], [52]. Nevertheless, chlorination remains the dominant water treatment method around the world, which is mainly because of the difficult access to high-quality water resources and limited budget for full update of distribution networks. Contradictory results regarding the OBPs formation by UV/chlorine AOP were reported,

possibly due to the different UV fluences and water quality. The study of Wu et al. demonstrated that UV/chlorine treatment enhanced the formation of the four major OBPs (namely CF, CH, DCAN and TCNM) in the tested TMP solution, compared with dark chlorination [5]. Nevertheless, in the research of Yang et al., the OBPs levels (mainly THM, CH, HK, TCNM and HAN) in the river water samples after UV/chlorine oxidation were comparable or lower than those after chlorination alone, and there's no significant increase of OBPs found in UV/chlorine compared to UV/H_2O_2 with post-chlorination [53]. A pilot study of UV/chlorine for the removal of 2-methylisoborneol (an algal-derived taste and odor compound) found that the maximum instantaneous level of THM and HAA were 1.7 and 2 μg/L, respectively [32]. The THM concentration in the three-day simulated distribution system was between 27.2 and 45.6 μg/L in the same study, which was below the USEPA maximum contaminant level (80 μg/L) for the pilot conditions.

Therefore, for countries where chlorination is currently adopted, the existing evidence seems to support that the UV/chlorine process is still a rising AOP, especially in terms of efficacy and cost. It is noteworthy, however, that in most literature, UV/chlorine process was considered to be only effective at acidic pH [37], [39], [54], [55]. Thus, further verification of the efficacy of UV/chlorine AOP at alkaline pH is needed, and this wish to find wider treatment conditions for the application of UV/chlorine leads to the idea of varying the UV wavelength.

1.5 Light-emitting diodes (LEDs) as UV sources

LEDs are promising UV sources and have been considered to be able to replace the conventional UV lamps in water treatment industries in the near future [56]. LED-UVs can emit specific wavelength ranging from 210 to 410 nm by changing the material of LEDs [57]. Besides, they possess several other advantages such as friendly to environment and lower power consumption [58], which will be elaborated in section 2.2. Recently, LED-UV has also been applied in lab-scale AOP systems: in Kwon et al.'s study, the 275 nm LED-UV /chlorine system achieved a better performance than the 254 nm LP-UV/chlorine system at pH 8 on the degradation of both nitrobenzene and ibuprofen [59].

1.6 Study objective

Based on the background information above, the main objective for this project is:

To study the feasibility of UV/chlorine process for TMP removal over wider treatment conditions.

Therefore, in this study, the kinetics of TMP degradation by LED-UV/chlorine process with different wavelengths (265 nm, 275 nm, 310 nm) and different pHs were investigated. The results were compared with those of conventional low-pressure UV/chlorine (254 nm) process to evaluate the wavelength and pH effects on TMP degradation. For this comparative evaluation, the UV intensities of the four UV systems were measured, and the TMP removal efficiency was compared as a function of UV dose. The source of the UV light with the same wavelength has no effect on the photochemical decomposition of the micropollutants [59]. Then the effects of operation parameters including oxidant dosage and water matrix on TMP removal were also examined. Finally, the degradation intermediates of TMP during UV/chlorine oxidation were preliminarily studied.

Efforts were made to answer the following research questions:

- How does LED-UV/chlorine perform in terms of TMP degradation, compared with conventional LPUV/chlorine and dark chlorination?
- How does UV wavelengths affect the TMP degradation during UV/chlorine process?
- How does pH affect the TMP degradation during UV/chlorine process?
- How does the oxidant dosage affect the TMP degradation during UV/chlorine process?
- How does the presence of natural organic matter (NOM) in water affect the TMP degradation during UV/chlorine process?
- What are the possible degradation intermediates of TMP during UV/chlorine process?

2 Background knowledge

2.1 UV radiation

2.1.1 Types of UV radiation

Ultraviolet is a band of the electromagnetic radiation with a wavelength in between of visible light and X-rays. Figure 2-1 shows the major types of UV radiation classified according to their wavelengths. UV-A rays have the longest wavelength (315-400 nm), followed by UV-B (280-315 nm), UV-C (200-280 nm) and vacuum UV (100-200 nm) [60]. As the photon energy is inversely proportional to the wavelength, the photon energy of the four types of UV is 3.10-3.94 eV, 3.94-4.43 eV, 4.43-6.2 eV and 6.2-12.4 eV, respectively. The Sun emits UV light at all the four bands, however, about 99% of UV rays that reach the earth's surface is UV-A. Almost 100% of the UV-C rays and 95% of UV-B rays is filtered by the first ozone layer of the atmosphere, while the vacuum UV is strongly absorbed by atmospheric oxygen.

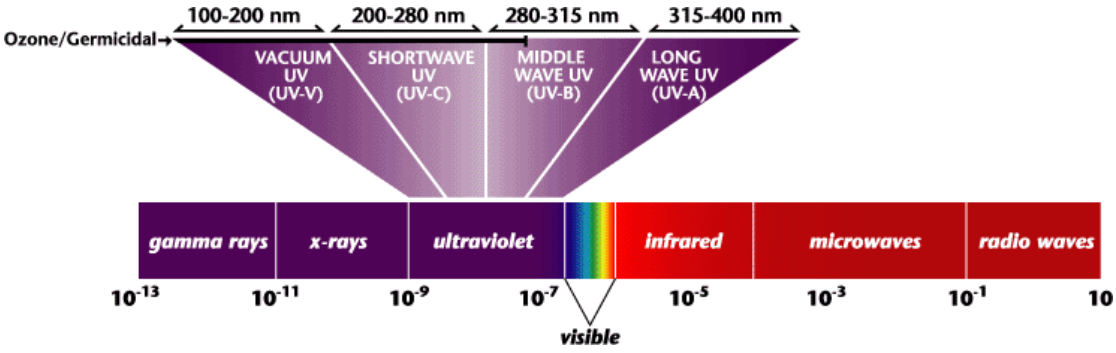

Figure 2-1: Electromagnetic Spectrum. Obtained from [61].

2.1.2 Conventional UV lamps

Currently, the major UV sources for UV system in water treatment plants are low- and medium-pressure mercury lamps.

The low-pressure UV lamps contain mercury gas with pressure ranging from about 100 to 1000 pa, which emit a monochromatic wavelength of 253.7 nm (254 nm) at high intensity when excited by an electrical charge. The 254 nm UV light is believed to have the maximum germicidal effect against microorganisms as it is in good agreement with the peak of DNA and RNA absorbance [62]. The output per lamp is between 30 to 600W with a wall plug efficiency (WPE, i.e. the ratio between the total radiometric optical output power, measured in Watts, and electrical input power) of 30-45%, normally. The life span of the lamp is ranging between 8000-16000 hours [63].

The medium-pressure UV lamps operate with mercury vapor pressure of approximately 10kPa, accordingly, the output of this type of lamp reaches 1-12 kW which is much higher than that of the low-pressure ones. They emit a broader range of wavelengths (200-600nm) at various intensities, which not only affect the DNA and RNA but also proteins and enzymes. It has been reported that the UV damage caused by low-pressure lamps can be repaired by microorganisms using certain enzymes, however, this kind of reactivation can hardly occur with polychromatic medium-pressure UV lamps [60]. The disadvantages of medium-pressure lamps are the relatively low power efficiency (10-15%) and short life span (4000 – 6000h) [63].

In general, even though the above two kinds of UV lamps are commonly applied for water purification, there are still some issue remained with them. One important concern is that they are fabricated with fragile quartz material and can pose a risk of mercury release [57]. Mercury is toxic and hazardous to public health and environment if not being disposed properly. Moreover, the operation of mercury lamps requires high drive voltage and electricity consumption. The relatively short life span and low WPE are also remaining challenges in practical application.

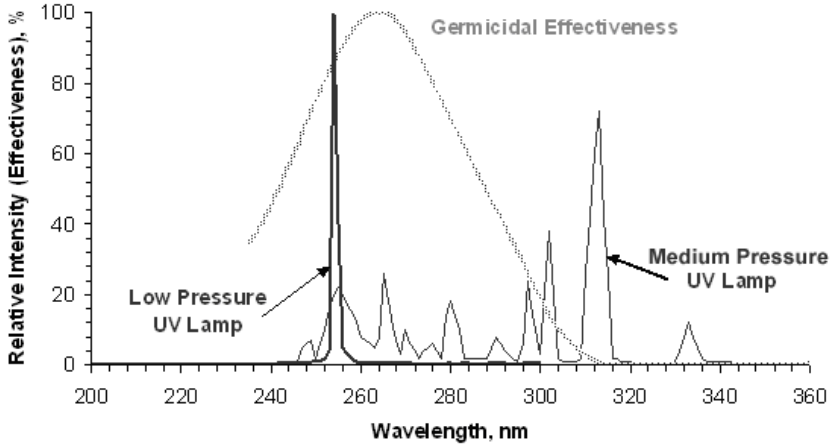

Figure 2-2: Spectral output of typical low- and medium-pressure UV lamp. Obtained from [64].

2.1.3 Determination of UV fluence

The fluence, or UV dose, is a measurement of the UV energy per unit area that is incident on a surface. It is calculated as the product of average UV intensity (I) and exposure time (t).

$$\text{fluence } (\text{mJ/cm}^2) = I\ (mW/cm^2) \times t\ (s)$$

Equation 2-1: UV dose equation

In the case of UV disinfection, the required fluence is largely dependent on the target pathogens in the water and is also affected by factors such as water quality (UV transmittance). Typically, a dose of 40 mJ/cm^2 is applied in DTPs to ensure at least a 4-log reduction (99.99%) of most

pathogenic microorganisms. As regards the application in AOPs, the UV dose can be hundreds or even thousands of mJ/cm^2 [30].

To determine the fluence, the average UV intensity (or irradiance, fluence rate) should be measured properly. Current methods for quantifying UV intensity include UV radiometer, chemical actinometry and biodosimetry [65].

Radiometers are easy-to-use instruments, which convert the detected incident irradiance into currents and read directly in units of mW/cm^2. However, radiometers are error prone when the beam is not perfectly collimated. In this case, the reading needs to be corrected by multiplying petri factor, divergence factor, etc. to obtain the average UV intensity in the water [66].

Biological dosimeters measure the UV dose by quantifying the biological response.

Chemical actinometry involves measuring the photon exposure over a defined wavelength range by the yield from a chemical reaction. An established chemical actinometer should meet the following requirements [67], [68]:

- The quantum yields should be accurately known for a wide range of wavelengths;
- The photochemical reaction should be reproducible;
- Both light absorbers and photoproducts should be thermally stable;
- The photoproducts should be photostable at the exposure wavelength.

Potassium ferrioxalate is the most popular actinometer, as it is simple to use and sensitive over a broad range of wavelengths (254 nm to 500 nm). The photochemical reaction is shown in Equation 2-2. The generated Fe^{2+} is complexed with o-phenanthroline and then measured via UV-visible absorption spectrometry [68].

$$2\mathrm{Fe}(C_2O_4)_3{}^{3-} + hv \rightarrow 2Fe^{2+} + 5C_2O_4{}^{2-} + 2CO_2$$

Equation 2-2: Generation of Fe^{2+} in photochemical reaction via potassium ferrioxalate

The amount of Fe^{2+} produced from one single measurement is calculated by Equation 2-3

$$Fe^{2+}(\mathrm{moles}) = \frac{(A_{510,sample} - A_{510,blank}) \times V_0}{\varepsilon_{510} \times V_1}$$

Equation 2-3: Equation to calculate amount of Fe^{2+} generated from photochemical reaction

Where:

A_{510} —— ***absorbance*** of the sample/blank at wavelength of 510 nm;

V_0 —— total irradiated volume, mL;

V_1 —— volume withdrawn at one time from the irradiated solution form complex, mL;

ε_{510} —— ***molar absorption coefficient*** of Fe(II)-o-phenanthroline complex at 510 nm, 11100 $M^{-1}cm^{-1}$.

The two terms in bold italic are vital for the description of UV-based processes:

Quantum yield (ϕ)

Quantum yield is the parameter expressing the fraction of the absorbed radiation employed for the photolytic decomposition reaction [67].

$$\phi = \frac{numbers\ of\ events\ (e.g. molecules\ changed, formed\ or\ destroyed)}{numbers\ of\ photons\ absorbed\ at\ certain\ wavelength}$$

Equation 2-4: Quantum yield

Molar absorption coefficient (ε)

The molar absorption coefficient is a measurement of how strongly a chemical species attenuates light at a given wavelength.

Beer-Lambert Law

$$A = \varepsilon \times b \times C$$

Equation 2-5: Beer- Lambert's law

Where A is the absorbance; ε is the molar absorption coefficient ($M^{-1}cm^{-1}$); b is the length of solution the light passes through (cm); and C is the concentration of the solution (mol/L).

The quantum yields for ferrioxalate actinometer is given by:

$$\phi_\lambda = \frac{moles\ of\ Fe^{2+}\ generated}{einsteins\ of\ UV\ absorbed\ at\ wavelength\ \lambda}$$

Equation 2-6: Quantum yield of ferrioxalate actinometer

The denominator of Equation 2-6 can also be calculated as:

$$einsteins\ of\ UV\ absorbed = \frac{P \times (1-R) \times t}{U_\lambda} = \frac{P \times (1-R) \times t}{\frac{h \times c}{\lambda} \times N_A}$$

Equation 2-7: Equation to calculate the amount of absorbed UV

where

P —— power of incident UV beam, W;

R —— reflection coefficient for incident beam;

t —— exposure time, s;

U_λ —— energy per Einstein at wavelength λ, J/Einstein;

h —— Planck constant, 6.62607004×10^{-34} m^2kg/s;

c —— speed of light, 2.99792458×10^{8} m/s;

N_A —— Avogadro number, 6.02214179×10^{23} mol^{-1}.

Given the above equations, the average UV intensity can be calculated using Equation 2-8.

$$I = \frac{\frac{d[Fe^{2+}]}{dt} \times h \times c \times N_A \times \phi_\lambda}{(1-R) \times \lambda \times s}$$

Equation 2-8: Average UV intensity via application of Ferrioxalate Actinometer

Where

$\frac{d[Fe^{2+}]}{dt}$ —— Fe^{2+}generation rate in the irradiated volume, mole/s;

s —— surface area of the irradiated water, cm^2.

2.2 LED as an UV light source

2.2.1 Light generation mechanism of LED

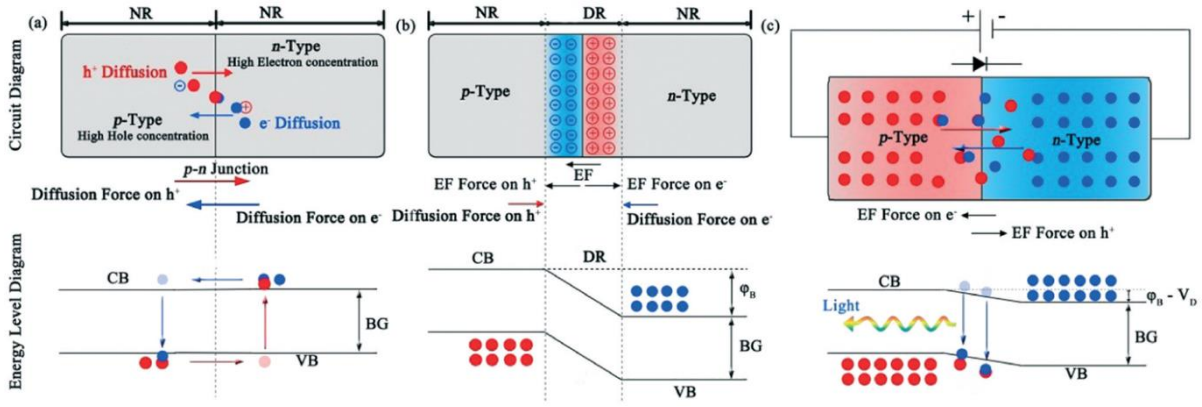

Figure 2-3: Light generation mechanism of LED. Where (a) depicts initial movement of mobile carriers at p-n conjunction; (b) equilibrium; (c) light emitting when bias voltage is applied. Obtained from[57].

UV-LEDs are devices comprising of solid-state semiconductor that convert direct current (DC) into electromagnetic waves in the UV wavelength range. The core component of a UV-LED is the p-n junction, which is formed when a p-type semiconductor is joined to an n-type semiconductor. The p-region is formed by doping a hole (i.e. h^+, positive charged carriers). To form a hole, Group II elements like Magnesium (Mg) are substituted as an impurity into a Group

III element (i.e., Ga or Al in AlGaN). Since the impurity has one less electron in its valence shell compared to Group III elements, holes are generated. Similarly, the n-region is formed by generating a free electron (i.e. e−, negative charge carriers). To generate a free electron, Group IV elements like Silicon (Si), holding one additional valence electron are substituted into a Group III element as an impurity. Due to the presence of a concentration gradient, the holes on the p-side and the electrons on the n-side diffuse toward the p-n junction, resulting in negative charges on the p-region, positive charges on the n-region and a potential energy difference (φ_B) between both sides. This forms a depletion region (DR) lacking of mobile charge carriers. An electric field is also created which prevents the diffusion of both charge carriers at equilibrium [57].

Once a bias voltage is applied, the voltage difference (V_D) can break the equilibrium and offset part of the φ_B. As current flows from the p- to n-region (as indicated by the polarity), there is a counter flow of electrons in the opposite direction. When electrons in the n-region conduction band (CB) combine with holes in the p-region valence band (VB), excess energy equivalent to the bandgap (i.e. the difference in energy levels between the conduction band and the valence band) is released in the form of light and heat. The amount of the released energy, as well as the wavelength of the light being emitted is determined by this bandgap, which is an intrinsic property of semiconductors. In other words, the emission wavelength can be tuned by changing the materials of semiconductors [57].

2.2.2 Characteristics of UV-LED

To date, the most frequently used UV-LED materials are based on diamond (235 nm) and Group III-nitride, including boron nitride (BN, 215nm), aluminum nitride (AlN, 210nm), gallium nitride (GaN, 365nm), indium gallium nitride (InGaN, 365-410nm), aluminum gallium nitride (AlGaN, 210-365nm) and AlInGaN (down to 210 nm) [57]. The output UV wavelength is dependent on the ratio of Al, Ga and In in the material: a higher molar fraction of Al results in a shorter wavelength whereas a higher fraction of In leads to a longer wavelength.

As an emerging UV light source, the UV-LED has several attractive advantages over conventional UV lamps [58], [69]:

- Mercury free, no risk of chemical leaching;
- Monochromatic emission at any specific wavelength;
- High frequency switch;
- Instant start (no warm-up period);
- Longer lifetime (achieved for UVA/UVB-LEDs, predictable for UVC-LEDs);
- More durable shell material (mental or ceramic);

- Small chip sizes enable the flexibility in LED array and reactor design;
- Lower operation temperature;

Despite all these present advantages, relatively low WPE and low output power are still major limitations for implementing the usage of UV-LEDs in water treatment technologies. Besides, the capital cost of UV-LEDs is much higher than traditional lamps, especially UVC-LEDs [58]. Generally, the trend is as follows —— the lower the wavelength, the higher the LED cost. Nevertheless, based on the developmental history of LED technologies, researchers predicted that the wall-plug efficiency of UV-LEDs can reach up to 75% with a lifetime over 100,000 hours by 2020 and the cost will also reduce significantly [70]. As UV-LED technology becomes more and more economically viable, the global UV-LED market size is expected to grow from 259.8 million US dollar in 2017 to 1163.5 million by 2023, and the UV-LED market is expected to shift from one that is UVA-dominated to UVC-dominated in the coming years.

2.2.3 Application of UVLEDs in AOPs

In recent years, UV-LEDs with various wavelengths have been applied in lab-scale advanced oxidation systems to remove organic pollutants from water. Among those, UVA-LED/TiO_2-based photocatalysis have been studied most frequently; while UVB- and UVC-LEDs have been used more in UV/H_2O_2, photo-Fenton and UV/persulfate processes [69]. There's one paper published in 2016 investigated the performance of LED UV/chlorine process on the degradation of carbamazepine (CBZ), one pharmaceutical commonly detected in WWTPs. The results revealed that the LED UV/chlorine process achieved a CBZ degradation rate almost 10 times higher than the LED UV/H_2O_2 process, at an oxidant dosage of 0.28mM, under LED-UV radiation of both 280 nm and 310 nm [49]. In a more recent research, the degradation of both nitrobenzene and ibuprofen by the 275 nm LED-UV /chlorine system was faster than by the 254 nm LP-UV/chlorine system at pH 7 and pH 8 [59].

The existing studies are limited in lab scale and synthetic water, or even distilled water, so there is still a long way to go for the real-world application.

2.3 Chlorine photolysis

2.3.1 Radical formation

In the normal pH range of natural waters (6.0~8.5), free chlorine exists mainly as an equilibrium mixture of hypochlorous acid (HOCl) and its conjugate base hypochlorite (ClO^-), with a pK_a of around 7.5 [71]. Both species can react with numerous organic and inorganic micropollutants, partially due to their high oxidation potentials ($E^0_{HOCl} = 1.45, E^0_{OCl^-} = 0.97$) [32].

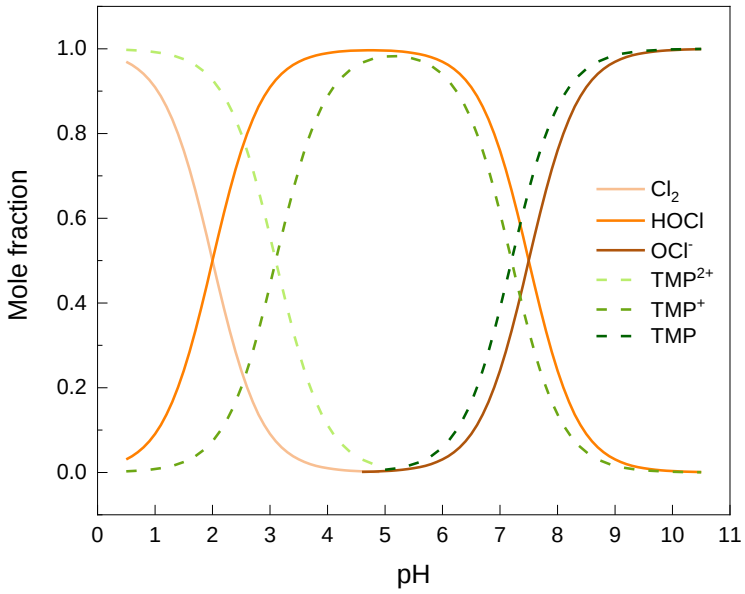

Figure 2-4: Chlorine and TMP speciation as a function of pH.

During UV photolysis of free chlorine, hydroxyl radicals ($\bullet OH$ /$\bullet O^-$) and chlorine atoms ($Cl\bullet$) are produced primarily (R2-3). $Cl\bullet$ reacts with chloride to form $Cl_2^{-\bullet}$ (R15), and both $Cl\bullet$ and $\bullet OH$ can react with $HOCl/OCl^-$ to generate $ClO\bullet$ (R8-9, R11-12). The major reactions involved in the chlorine photolysis are summarized in Table 2-1.

$\bullet OH$ is deemed as the most important radical in most AOPs. It is a non-selective oxidant with the redox potential of 2.80V [72] and are capable of reacting with various organic compounds at nearly diffusion-controlled rates. On the other hand, this also means that other components in water matrix, like NOM and bicarbonate, will compete with target pollutants for $\bullet OH$ radical. Reactive chlorine species (RCS) such as $Cl\bullet$, $Cl_2^{-\bullet}$ and $ClO\bullet$ are selective radicals with oxidation potential of 2.4, 2.0 and 1.5-1.8V, respectively [73]. Their contributions to the decomposition of different PPCPs depend more on the chemical structures of the compounds. $Cl\bullet$ can react rapidly with compounds like phenol, benzoic acid and chlorobenzene; whereas $Cl_2^{-\bullet}$ and $ClO\bullet$ are more reactive to aromatics containing methoxy groups. $Cl_2^{-\bullet}$ can also react fast with olefinic compounds and aromatics when the ring is substituted with hydroxy and amino groups [72].

Table 2-1: Summary of major reactions in the UV/chlorine system. Adapted from [14], [30], [34].

No.	Reactions	Rate constant, quantum yield and pKa
R1	$HOCl \rightleftharpoons H^+ + OCl^-$	$pk_{a1} = 7.4\sim7.47$
R2	$HOCl + hv\ (\lambda < 400) \rightarrow \bullet OH + Cl\bullet$	$\phi_{HOCl,254} = 1.0\sim2.8\ mol/Es$ $\phi_{\bullet OH,254} = 1.4\ mol/Es$
R3a	$OCl^- + hv\ (\lambda < 320) \rightarrow \bullet O^- + Cl\bullet$	$\phi_{OCl^-,254} = 0.85\sim2.4\ mol/Es$ $\phi_{\bullet OH,254} = 0.278\ mol/Es$
R3b	$OCl^- + hv\ (\lambda < 320) \rightarrow O(^1D) + Cl^-$	$\phi_{O(^1D),254} = 0.133\ mol/Es$
R3c	$OCl^- + hv\ (\lambda > 320) \rightarrow O(^3P) + Cl^-$	$\phi_{O(^3P),254} = 0.074\ mol/Es$
R4	$\bullet OH \rightleftharpoons H^+ + \bullet O^-$	$pk_{a4} = 11.9 \pm 0.2$
R5	$O(^1D) + H_2O \rightarrow 2 \bullet OH$	$k_5 = 1.2 \times 10^{11}\ M^{-1}s^{-1}$
R6	$O(^3P) + O_2 \rightarrow O_3$	$k_6 = 4 \times 10^9\ M^{-1}s^{-1}$
R7	$O(^3P) + OCl^- \rightarrow ClO_2^-$	$k_7 = 9.4 \times 10^9\ M^{-1}s^{-1}$
R8	$\bullet OH + HOCl \rightarrow ClO\bullet + H_2O$	$k_8 = 8.5 \times 10^4\sim2.0 \times 10^9\ M^{-1}s^{-1}$
R9	$\bullet OH + OCl^- \rightarrow ClO\bullet + OH^-$	$k_9 = 8.8 \times 10^8\sim9.8 \times 10^9\ M^{-1}s^{-1}$
R10	$\bullet OH + Cl^- \rightarrow HOCl^{-\bullet}$	$k_{10} = 4.3 \times 10^9\ M^{-1}s^{-1}$
R11	$Cl\bullet + HOCl \rightarrow ClO\bullet + H^+ + Cl^-$	$k_{11} = 3 \times 10^9\ M^{-1}s^{-1}$
R12	$Cl\bullet + OCl^- \rightarrow ClO\bullet + Cl^-$	$k_{12} = 8.2 \times 10^9\ M^{-1}s^{-1}$
R13	$Cl\bullet + OH^- \rightarrow HOCl^{-\bullet}$	$k_{13} = 1.8 \times 10^{10}\ M^{-1}s^{-1}$
R14	$Cl\bullet + H_2O \rightarrow HOCl^{-\bullet} + Cl^-$	$k_{14} = 3.0 \times 10^2\sim1.8 \times 10^5\ M^{-1}s^{-1}$
R15	$Cl\bullet + Cl^- \rightarrow Cl_2^{-\bullet}$	$k_{15} = 6.5 \times 10^9\sim2.1 \times 10^{10}\ M^{-1}s^{-1}$
R16	$Cl_2^{-\bullet} \rightarrow Cl\bullet + Cl^-$	$k_{16} = 6.0 \times 10^4\sim1.1 \times 10^5\ s^{-1}$
R17	$Cl_2^{-\bullet} + OH^- \rightarrow Cl^- + HOCl^{-\bullet}$	$k_{17} = 7.3 \times 10^6\sim4.5 \times 10^7\ M^{-1}\ s^{-1}$
R18	$Cl_2^{-\bullet} + H_2O \rightarrow Cl^- + HOCl^{-\bullet} + H^+$	$k_{18} = 24\ M^{-1}\ s^{-1}$
R19	$HOCl^{-\bullet} \rightarrow \bullet OH + Cl^-$	$k_{19} = 6.1 \times 10^9\ M^{-1}s^{-1}$
R20	$HOCl^{-\bullet} \rightarrow Cl\bullet + OH^-$	$k_{20} = 23\ s^{-1}$
R21	$HOCl^{-\bullet} + H^+ \rightarrow Cl\bullet + H_2O$	$k_{21} = 21\ M^{-1}\ s^{-1}$
R22	$HOCl^{-\bullet} + Cl^- \rightarrow Cl_2^{-\bullet} + OH^-$	$k_{22} = 1.0 \times 10^5\ M^{-1}s^{-1}$
R23	$O_3 + ClO_2^- \rightarrow ClO_2 + O_3^{-\bullet}$	$k_{23} = 4.0 \times 10^6\ M^{-1}s^{-1}$

2.3.2 Photodecomposition rate

- Chlorine photodecomposition rate

The decomposition rate of chlorine with UV exposure has been reported to be wavelength- and pH-dependent. The empirical model established by Yin et al. [56] showed that the photodecay rate of chlorine increased with wavelength at pH 5~10, and with pH in the studied wavelength range (257.7-301.2nm) (refer to Figure 2-5). In another research [74], the chlorine photolysis was found to be faster at 275 nm in neutral and alkaline environment (pH≥7.0), comparing to 254 nm and 310 nm (refer to Figure 2-6).

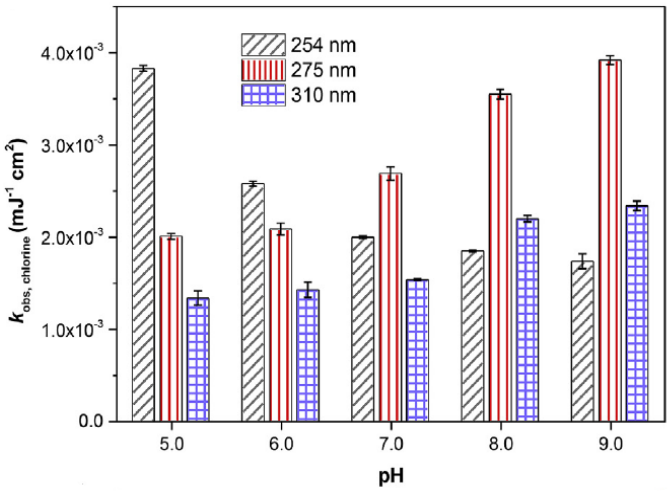

Figure 2-6: Measured results ([chlorine]$_0$=14.2 mg/L as Cl2, [DOC]$_0$=3.0mg C/L) from [36].

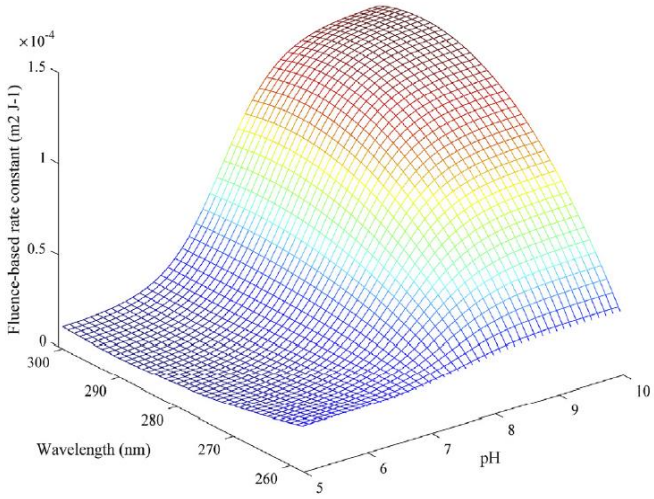

Figure 2-5: Reported wavelength and pH effects on fluence-based rate constant of chlorine photodecomposition.

- Molar absorption coefficient

The wavelength-dependency of chlorine photolysis could be partially attributed to the variation of absorptivity of HOCl/OCl^- with changing wavelength. As shown in Figure 2-7, HOCl has a maximum absorption coefficient of 98~101 $M^{-1}cm^{-1}$ at 236 nm, whereas ClO^- gets its peak value of approximately 365 $M^{-1}cm^{-1}$ at 292 nm [46], [75]. Both species have similar absorption coefficients (~ 60 $M^{-1}cm^{-1}$) at 254nm.

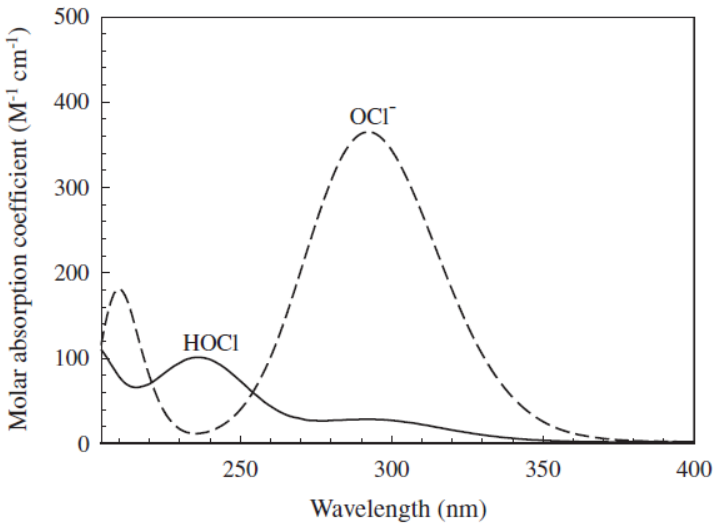

Figure 2-7: Absorption spectra of HOCl and OCl^-. measured respectively at pH 5 and pH 10. Obtained from [37].

➢ Quantum yield

The quantum yield of HOCl/OCl^- is always calculated using measured molar absorption coefficient and photodecomposition rate. The two types of quantum yields mentioned in Table 2-1 are the quantum yield of chlorine loss (Equation 2-9), and the quantum yield of •OH formation (Equation 2-10). The latter one is considered as the true quantum yield of reaction R2 and R3a. The former one, also called apparent quantum yield, is often greater than 1 owing to the destruction of HOCl/OCl^- via subsequent radical reactions (e.g. R8, R9, R11 and R12) [39], [46]. The quantum yields used in this report always refer to the quantum yields of chlorine loss.

$$\Phi_{HOCl(OCl^-)} = \frac{moles\ of\ free\ chlorine\ decomposed}{einsteins\ of\ photons\ absorbed\ \ at\ certain\ wavelength}$$

Equation 2-9: Quantum yield of chlorine loss

$$\phi_{\bullet OH} = \frac{moles\ of\ \ \bullet OH\ generated}{einsteins\ of\ photons\ absorbed\ \ at\ certain\ wavelength}$$

Equation 2-10: Quantum yield of •OH formation

The quantum yields of chlorine at 254nm has been widely studied by researchers, as listed in Table 2-1, $\Phi_{HOCl,\ 254}$ = 1.0~2.8 mol/Es, and $\Phi_{OCl^-,254}$ = 0.85~2.4 mol/Es. However, limited literature focused on the quantum yields of chlorine at higher wavelength. Based on Yin et al.'s study (Figure 2-8) [56], the quantum yields of both species decreased as wavelength increased from 257.7 nm to 301.2 nm and the quantum yield of HOCl was higher than that of ClO^- at the same wavelength.

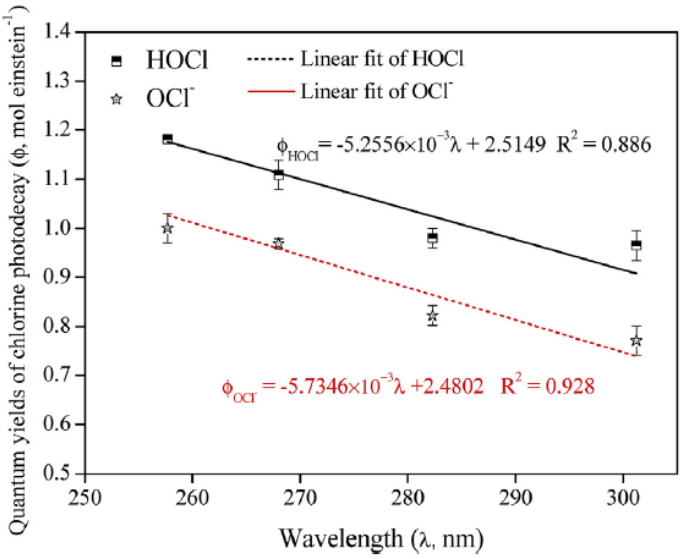

Figure 2-8: Apparent quantum yields of HOCl and OCl^- photodecay as a function of wavelength. ($[chlorine]_0$=100 μM). Obtained from [35].

2.4 Photochemical properties of TMP

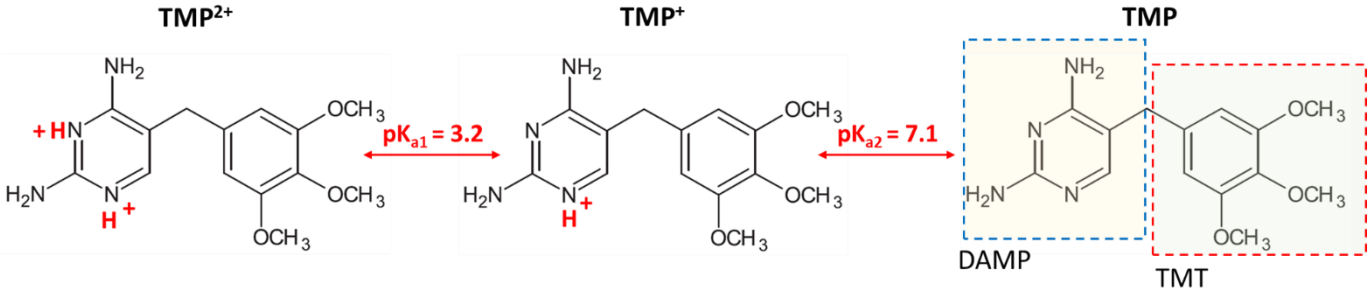

Figure 2-9: Structure and speciation of TMP [39]

The structure of TMP is relatively complex, with two sub-structural moieties of TMP: 2,4-diamino-5-methylprimidine (DAMP) and 3,4,5-trimethoxytoluene (TMT). It possesses benzene rings, pyrimidine, alkyl, amine and methoxyl groups. TMP is known to have two pK_a values due to protonation of the pyrimidine group. (pK_{a1}=7.1, pK_{a2}=3.2).

Though the UV absorption coefficient of TMP in aqueous solution reaches up to 3500 $M^{-1}cm^{-1}$ at 254nm, the quantum yield of TMP is rather low, indicating its low degradation rate under UV irradiation.

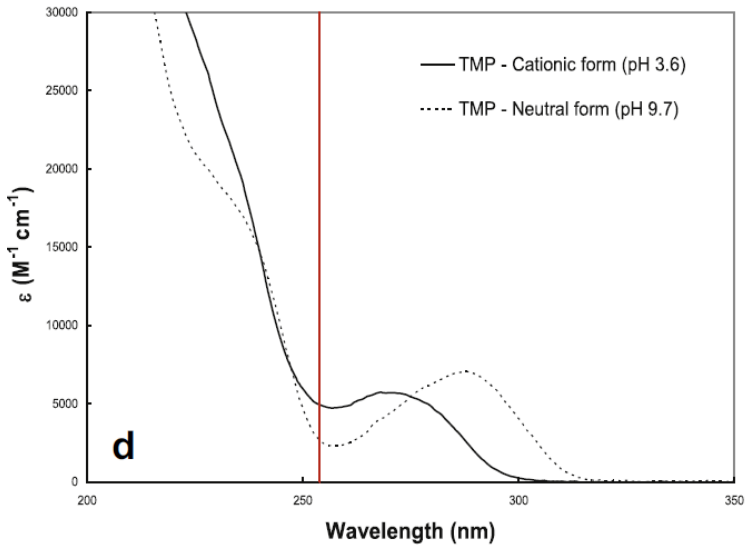

Figure 2-10: UV absorption spectrum of TMP as a function of UV wavelength in aqueous phase. Obtained from [40]

Table 2-2: Absorption coefficients and quantum yields of TMP at 254nm. Adapted from [40]

pH	**3.6**	**7.85**	**9.7**
Absorption coefficient ε ($M^{-1}cm^{-1}$)	4956	2942	2635
Quantum yield Φ (mol/Es)	$5.9\ (\pm 2.9)\times 10^{-4}$	$1.18(\pm 0.11)\times 10^{-3}$	1.49×10^{-3}

3 Materials and methods

3.1 Chemicals and solution preparation

3.1.1 Reagents

All solutions were prepared using reagent-grade chemicals and deionized water (18.2MΩcm) produced by a Milli-Q water purification system (Thermo Scientific, SG). TMP (⩾98%, TLC), sodium hypochlorite solution (NaClO, available chlorine 10-15%), sodium thiosulfate ($Na_2S_2O_3$) and humic acid were purchased from Sigma-Aldrich (US). Methanol and formic acid of LCMS grade were purchased from Fisher Chemical (SG) and Sigma-Aldrich (US), respectively.

The following chemicals used for ferrioxalate actinometry experiments: ferric sulfate hydrate ($Fe_2(SO_4)_3$, 97%), potassium oxalate monohydrate ($K_2C_2O_4 \cdot H_2O$, 99%), sodium acetate ($CH_3COONa \cdot 3H_2O$, 99%), 1,10-Phenanthroline (99%), hydroxylamine hydrochloride ($NH_2OH{\cdot}HCl$, 99%) and sulfuric acid (H_2SO_4, 95%-98%) were purchased from Sigma-Aldrich (US).

3.1.2 Solution preparation

- TMP solution

The TMP stock solution (400 mg/L) was prepared by adding the pure TMP powder to deionized water and stirring overnight.

- Free chlorine

The chlorine dosage ranged from 0.3 to 6 mg/L in this study. For concentrations higher than 1mg/L, the NaClO stock solution was added into the buffered TMP solution directly; while for lower concentrations, the NaClO stock solution was diluted right before each use.

- Buffers

The buffer solutions consisted of monobasic (KH_2PO_4) and dibasic potassium phosphate (K_2HPO_4). By varying the amount of each salt, a pH range of 6.0-9.0 was obtained. The values in Table 3-1 were calculated using the Henderson-Hasselbalch equation (Equation 3-1) [76] and a mass balance. The phosphate would not affect the experimental results in this study as it has no significant impacts on the concentrations of ·OH or reactive chlorine species [56].

$$\mathrm{pH} = \mathrm{pK}_a{}' + log\frac{[basic\ species]}{[acidic\ species]} \quad (where\ \mathrm{pK}_a{}' = 6.86\ at\ 25\ ℃)$$

Equation 3-1: Henderson-Hasselbalch Equation

Table 3-1: Preparation of 0.1M Potassium phosphate buffer (1L) at 25℃

pH	KH_2PO_4 (g)	K_2HPO_4 (g)
6.0	11.96	2.11
7.0	5.72	10.10
8.0	0.92	16.24
9.0	0.10	17.30

- Quencher

Quenching is a term to describe the introduction of a material that combines with any unused reactants and effectively stops a reaction. In this study, sodium thiosulfate ($Na_2S_2O_3$) was selected as a quencher to consume the residual free chlorine in the samples. The $Na_2S_2O_3$ solution was prepared weekly. The reaction between $Na_2S_2O_3$ and NaClO is:

$$4NaClO + Na_2S_2O_3 + 2NaOH \rightarrow 4NaCl + 2Na_2SO_4 + H_2O$$

Equation 3-2: Quenching equation between $Na_2S_2O_3$ and NaClO

- Humic acid solution

The humic acid stock solution (1000 mg/L) was prepared by dissolving solid humic acid into deionized water and stirring overnight.

3.2 UV irradiation

3.2.1 Experimental set-ups

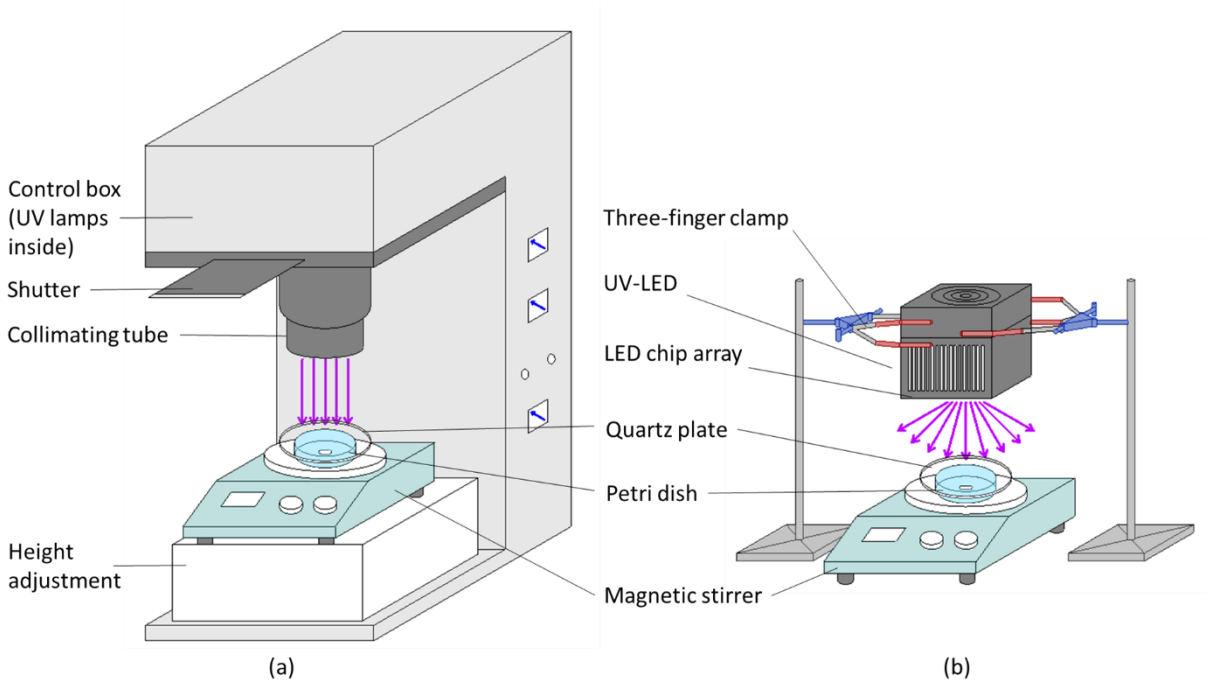

Figure 3-1: Schematic diagram of experimental set-ups. (a) UV quasi-collimated beam system (254 nm); (b) UV-LED system (265/275/310 nm)

Figure 3-1 shows the schematic diagram of the experimental set-ups used in this study. The monochromatic 254 nm low-pressure UV lamp (10W, Calgon Carbon Corporation, US) was placed in a quasi-collimated beam apparatus; while the UV-LED 265/275/310 (Taoyuan Electron, Hongkong) was fixed by two three-finger clamps. The LED chip array on the front of the UV-LED device is shown in Figure 3-2. The distance from the chip array to the solution surface was 10.2 cm.

3.2.2 UV intensity measurement

Considering the divergence of the LED-UV beam, this study chose ferrioxalate as an actinometer to measure the UV intensity in the reactor (irradiation area of 24.63 cm^2 and solution depth of 0.81 cm). The detailed procedures of actinometry experiments can be found in one study by Bolton et al. [68]. The UV intensity values was calculated from the quantum yields of 1.38 at 254 nm [68] and 1.24 at 265, 275 and 310 nm [77]. The determined average UV intensities at the solution surface were listed in Table 3-3.

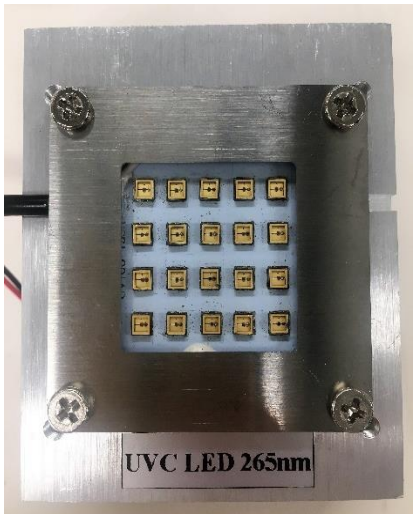

Figure 3-2: LED chip array

Table 3-2: Parameters of UV-LEDs (T=25℃, IF=600 mA)

	UVLED 265	**UVLED275**	**UVLED310**
Peak emission wavelength	265 nm	275 nm	310 nm
Power range	60-80 mW	80-100 mW	60-80 mW
Voltage range	10-15 V		
Light-emitting angle	120°		
Number of chips	20 (5×4)		
Mechanical dimensions	L78 × W68 × H68 mm		
Heat dissipation method	Air cooled		
Service life	> 8,000 h	> 10,000 h	> 10,000 h

Table 3-3: Average UV intensity of the four UV systems

Device	**LP-UV 254**	**LED-UV 265**	**LED-UV 275**	**LED-UV 310**
UV intensity (mW/cm^2)	0.2467	0.1774	0.2564	0.1769

3.3 Experimental procedures

Figure 3-1 shows the 4 UV irradiation systems in this study. The 254nm LPUV lamp (Figure 3-1(a)) was warmed up for 5 min before experiments, while the experiments conducted with

the other three systems (Figure 3-1(b)) started instantly once the switch was on.

All kinetics experiments were conducted in a 20mL petri dish containing 200 μg/L TMP solution. The solution was magnetically stirred at 150 rpm and covered with a quartz plate to prevent evaporation. The reaction pH value was adjusted to 6, 7, 8 or 9 using 2mM phosphate buffer. The testing solution was spiked with NaClO solution to give an initial free chlorine concentration of 0.3 – 6 mg/L and simultaneously exposed to the monochromatic UV light at one of the four wavelengths (254/265/275/310) each time. Samples (0.5mL) were collected at pre-determined time intervals and the residual free chlorine was quenched with $Na_2S_2O_3$ at 4 times of stoichiometric ratio. Control tests of TMP degradation by UV photolysis alone and dark chlorination were carried out in a similar manner, but in the absence of chlorine and UV light, respectively. To evaluate the effect of NOM on TMP removal, different concentrations of humic acid solution was spiked into the testing solution. Samples containing humic acid were filtered through 0.45-μm filter membranes before being added into the LC-MSMS vials.

To identify potential degradation intermediates during TMP degradation by the UV/chlorine process, higher initial concentrations of TMP (10 mg/L) and chlorine (15 mg/L) were used. After a certain reaction time in each run, the reaction was quenched by $Na_2S_2O_3$ and a 0.5mL sample was collected.

TMP kinetics experiments were conducted at least in triplicate. All experiments were carried out at room temperature (around 22℃).

3.4 Analytical methods

3.4.1 Experimental analysis

The concentration of free chlorine in NaClO stock solution was periodically standardized by diethyl-p-phenylene-diamine (DPD) colorimetry [78]. The total organic carbon (TOC) level of HA solutions were measured by a TOC analyzer (Shimadzu, Japan). The solution pH was measured with a pH meter (Schott, SG).

The concentration of TMP was determined by a high performance liquid chromatography-double mass spectrometry (HPLC-MS/MS) system (8030, Shimadzu, Japan) equipped with a Shim-pack FC-ODS column (150×2 mm, particle size 3 μm) at 40 ℃. The mobile phase for the measurement consisted of 0.1% formic acid (A) and methanol (B), at a flow rate of 0.3 mL/min. The sample injection volume was 10 μL. The gradient program of HPLC was as follows (A/B, v/v%): 90/10 (0-1min), decreasing linearly to 10/90 (1-4min), 10/90 (4-8min), increasing linearly to 90/10 (8-8.1min) and 90/10 (8.1-10min). During 1-4min and 8-8.1min,

the value changed linearly with time. The LC was coupled to the MS using electrospray ionization (ESI) in positive mode. Multiple reaction monitoring (MRM) was applied to quantify the protonated product ($[M+H]^+$) with Q1 mass of 291.20 and Q3 mass of 230.10. Under the optimized condition, the retention time for TMP was 4.53 min.

For elucidation of the degradation products, the gradient program (A/B, v/v%) was changed to 60/40 (0-1 min), decreasing linearly to 5/95 (1-5.5 min), 5/95 (5.5-7.0 min), increasing linearly to 60/40 (7.0-7.1 min) and 60/40 (7.1-12 (30) min). The samples were fully scanned over the m/z range of 100-450.

3.4.2 Data analysis

For a typical second-order reaction, the rate of disappearance of one reactant is:

$$\frac{dA}{dt} = -k''[A][B]$$

Equation 3-3: Differential equation of second-order kinetic reaction(s)

where k'' is the second-order rate constant of A reacting with B. If the concentration of B is constant or [B]>>[A], Equation 3-3 can be simplified to:

$$\frac{dA}{dt} = -k'[A]$$

Equation 3-4: Differential equation of pseudo-first-order kinetic reaction(s)

The integrated form of Equation 3-4 is:

$$\ln\frac{[A]}{[A]_0} = -k't$$

Equation 3-5: Equation of pseudo-first-order kinetic reaction(s) expressed as a ratio of the concentration of A

where k' is the pseudo-first-order rate constant.

The kinetics of photolytic decomposition of organic compounds is usually fitted by the pseudo-first-order kinetics model [79]. In this study, the $\ln([TMP]/[TMP]_0)$ over time was plotted. Besides, for a constant UV intensity, the $\ln([TMP]/[TMP]_0)$ was hypothesized to be proportional to the UV fluence, thus $\ln([TMP]/[TMP]_0)$ against UV fluence was also plotted.

4 Results and discussions

4.1 Degradation kinetics

4.1.1 TMP degradation by LP-UV alone, dark chlorination and LP-UV/chlorine

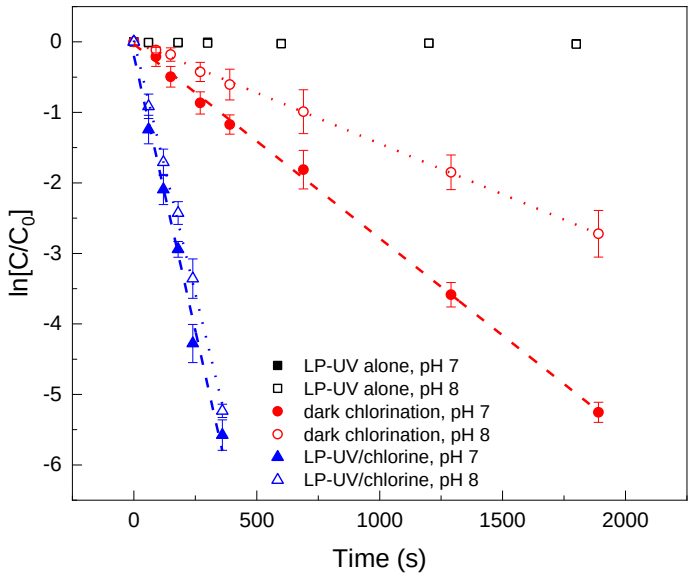

Figure 4-1: Comparison of TMP degradation by LP-UV alone, dark chlorination and LP-UV/chlorine process. Condition: UV intensity: 0.2467 mW/cm^2, [TMP]$_0$=200 µg/L, [chlorine]$_0$= 3 mg/L as Cl_2.

Figure 4-1 depicts the degradation of TMP over time by LP-UV photolysis, dark chlorination and LP-UV/chlorine process at pH 7 and pH 8. C and C_0 were the concentrations of TMP at the sampling time and initial time, respectively. For direct UV photolysis, no obvious change of TMP concentration (~3% removal) was observed during the experiments. The dark chlorination achieved a TMP removal of 99% at pH 7 within 30 min, while the similar removal was obtained at 5 min by incorporating UV and chlorine. The UV/chlorine process significantly enhanced the degradation rate of TMP compared with dark chlorination and UV alone. Plots of ln[C/C_0] over time remained linear for both chlorination and UV/chlorine process, confirming that the TMP degradation followed the pseudo-first-order kinetics model. The pseudo-first-order rate constants k'were 2.78 (±0.25)×10^{-3} s^{-1}, 1.44 (±0.19)×10^{-3} s^{-1}, 1.56 (±0.10)×10^{-2} s^{-1} and 1.42 (±0.15)×10^{-2} s^{-1} for dark chlorination at pH 7&8 and UV/chlorine at pH 7& 8, respectively.

The low photodecomposition rate of TMP can be explained by its low quantum yield. The quantum yield Φ_{254nm} of TMP was previously reported to be 1.18 (±0.11)×10^{-3} mol/Es at pH 7.85 [80], resulting in a fairly low photolysis efficiency, despite of the relatively high molar absorption coefficient, which was 2942 M^{-1}cm^{-1} [80]. The k' values for UV/chlorine process

reached 5~10 times of those for dark chlorination in this study, which can be attributed to the generation of reactive oxidant radicals such as •OH, •Cl, $Cl_2^{-\bullet}$ and ClO• from chlorine photolysis [5], [47], [73]. This finding is basically in line with the observation of Wu et al.'s study [5], where the k' values of TMP degradation by chlorination and UV/chlorine were 3.37 (±0.15)×10^{-3} s^{-1} and 9.84 (±0.16)×10^{-3} s^{-1}, respectively.

4.1.2 Effect of wavelength

- Direct UV photolysis

As can be seen in Figure 4-2, changing of wavelength had no obvious effect on the UV photolysis efficiency of TMP. Besides, the minor removal of TMP indicates that the TMP cannot be effectively removed by UV system alone in water treatment plants.

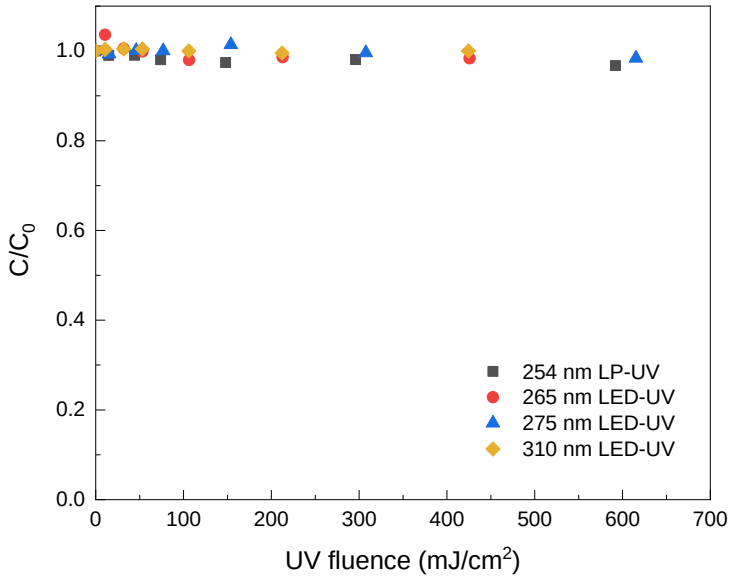

Figure 4-2: Direct UV photolysis of TMP with different wavelengths. Condition: $[TMP]_0$=200μg/L, pH 8

- UV/Chlorine process

The fluence-based pseudo-first-order rate constant k_f' was used instead of time-based rate constant k' when the 4 UV devices with various intensity values were discussed together. Figure 4-3 exhibited the degradation of TMP as a function of UV fluence at four different wavelengths at pH 8. To achieve a ~99% removal of TMP, the UV fluence values required for 254 nm, 265 nm, 275 nm and 310 nm were 89 mW/cm^2, 27 mW/cm^2, 22 mW/cm^2 and 52 mW/cm^2, respectively. The fluence-based pseudo-first-order rate constant was decreased in the order of 275nm > 265nm > 310nm > 254nm. The similar variation pattern was also observed in the case of pH 9 (Figure 4-6). However, the k_f' value for 254nm increased slightly as pH

decreased from 9 to 6. At pH 7, $k_{f,254}'$ was lower than $k_{f,265}'$ but higher than $k_{f,310}'$; while at pH 6 it was the highest among the four tested wavelengths (Figure 4-6). Collectively, UV light at 275 nm is the most efficient for TMP degradation at pH⩾7.

These results could be supported by the variation of chlorine photodecay rate at various wavelengths [74]. The decomposition rate of chlorine determines the radical formation during UV/chlorine process, and thus affect the removal rate of the target pollutant. As reported in previous research (Figure 2-6) [74], the fluence-based rate constant of chlorine decomposition at the wavelength of 275 nm was higher than 310 nm and 254 nm at neutral and alkaline pH; whereas for acidic pH (pH 5-6), the rate constant was highest at 254 nm followed by 275 nm and 310 nm [74]. According to Yin et al. [56], the molar absorption coefficient contributed more than the quantum yield of HOCl/OCl^- to the wavelength-dependent chlorine photolysis. So, for the three LED-UV wavelengths, even though the quantum yield at 265 nm is higher than that at 275 nm and 310 nm (Figure 2-8), the 275 nm system possesses the higher absorptivity (Figure 2-7) out of the 3 wavelengths, resulting in the fastest chlorine photodecay and thus the most rapid TMP degradation by UV/chlorine. Moreover, it should be noted that the effect of wavelength also depends on the pH of the solution, which will be discussed further in sections 4.1.3.

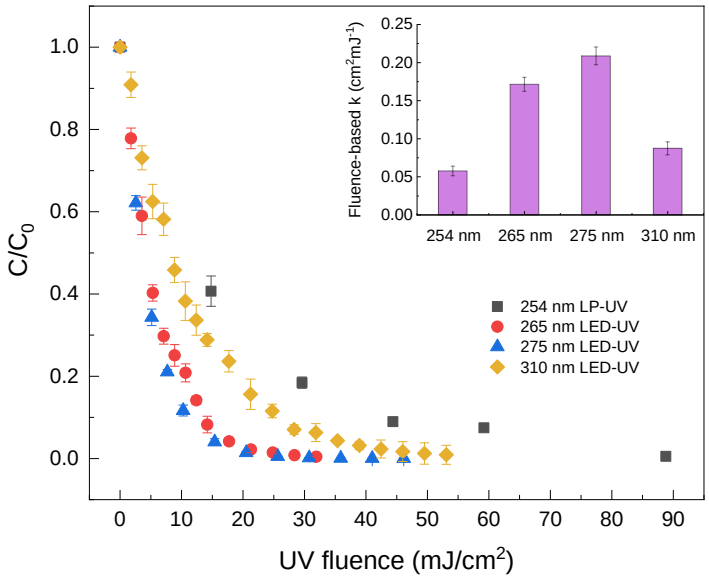

Figure 4-3: TMP degradation by UV/chlorine process with various wavelengths. Condition: $[TMP]_0$=200 µg/L, $[chlorine]_0$= 3 mg/L as Cl_2, pH 8

The results of this work were in accordance with a previous research where the degradation of nitrobenzene and ibuprofen by UV/chlorine was faster at wavelength of 275nm than 254 nm at pH 7 and pH 8 while the opposite was true at pH 6 [59]. Likewise, Wang et al. found that the

LED280 performed better than LED310 in the UV/chlorine system for the removal of carbamazepine in the pH range of 5.5-9.5 [49].

4.1.3 Effect of pH

- Dark chlorination

The performance of dark chlorination against TMP at various pH was compared in Figure 4-4. TMP was degraded by >99% at pH 7 in 40 min, while only 75% was removed at pH 9 at the same time. The pseudo-first-order rate constants of TMP reacting with free chlorine in descending order are: 2.8 (±0.2)×10^{-3} s^{-1} (pH 7), 1.4 (±0.2)×10^{-3} s^{-1} (pH 8), 1.1 (±0.1)×10^{-3} s^{-1} (pH 6) and 6.0 (±0.6)×10^{-4} s^{-1} (pH 9). This pattern of k' is in good agreement with the apparent second-order rate constant of TMP reacting with chlorine obtained in Dodd et al.'s study [78], where $k''_{app,TMP}$ increased from pH 5 to 7.5 and decreased when pH >7.5. The variation of k' in different pH conditions is probably because of the different reactivity amongst the individual acid-base species of TMP (pK_{a1}=3.2, pK_{a2}=7.1) and free chlorine (pK_a=7.5). According to Dodd et al.'s results [78], the second-order rate constant of HOCl reacting with TMP was the highest (16±1 $M^{-1}s^{-1}$) followed by that between HOCl and TMP^+ (6.2±1.2 $M^{-1}s^{-1}$), while the reactions among OCl^- and TMP species didn't contribute much to the overall reaction owing to the relatively low oxidation potential of OCl^-. Thereby, the whole reaction rate could reach the maximum where the mole fractions of both HOCl and neutral TMP are relatively high i.e. the intersection of the two lines representing HOCl and TMP respectively in Figure 2-4, which is at approximately pH 7.5. When the pH value gets larger, the OCl^- becomes the dominant species of chlorine; whereas when the pH is lower than 7.5, the mole fraction of neutral TMP decreased greatly due to protonation. Both cases would lead to the reduction of k' value, which could explain the different behaviors of dark chlorination on TMP degradation at pH 6~9 in this study.

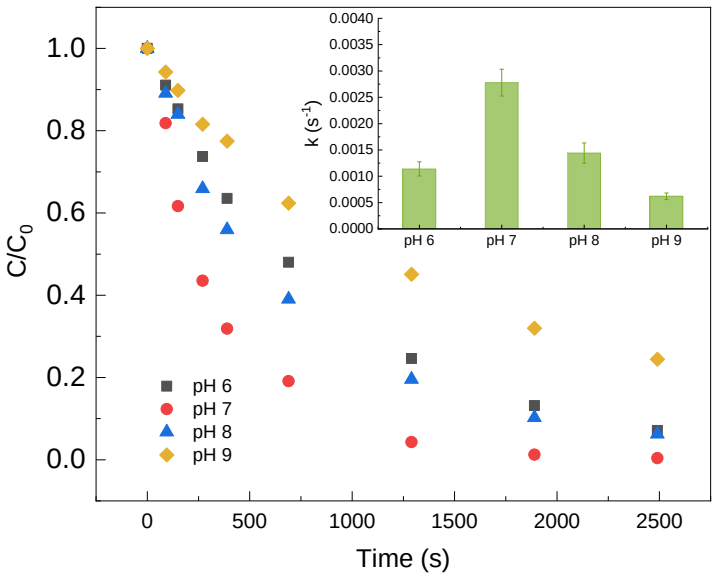

Figure 4-4: TMP degradation by dark chlorination at various pHs. Condition: $[TMP]_0$=200 μg/L, $[chlorine]_0$= 3 mg/L as Cl_2.

➢ UV/Chlorine process

The effect of pH on the TMP decomposition at the four studied wavelengths is shown in Figure 4-5 and Figure 4-6. The fluence-based rate constant at 265 nm, 275 nm and 310 nm increased greatly with the increasing pH. As for 265 nm and 275 nm, the k_f' values increased 5 times as pH was adjusted from 6 to 9 ($k_{f,265,pH6}'$ =0.032 ± 0.005 cm^2mJ^{-1}, $k_{f,265,pH9}'$ =0.21 ± 0.01 cm^2mJ^{-1}; $k_{f,275,pH6}'$ =0.048±0.004 cm^2mJ^{-1}, $k_{f,275,pH9}'$ =0.28±0.02 cm^2mJ^{-1}); while a tenfold increment was achieved by 310 nm ($k_{f,310,pH6}'$ =0.011±0.001 cm^2mJ^{-1}, $k_{f,310,pH9}'$ =0.13±0.02 cm^2mJ^{-1}). The variation of k_f' for 254 nm was totally different from the other three, with a reduction of 30% in k_f' from pH 6 to pH 9.

The pH affects the UV/chlorine process by influencing the HOCl/OCl^- speciation, which determines the absorbance and the quantum yields of chlorine photodecomposition and thus the radical production. Different radicals behave differently in the reactions with TMP, which finally leads to various TMP removal. This process can be further elaborated as follows:

(1) As pH increases from 6 to 9, the dominant chlorine species shifts from HOCl to OCl^-.
(2) The molar absorption coefficients of HOCl and OCl^- are almost identical at 254 nm, suggesting that the photolysis of chlorine is likely independent of pH at this wavelength [46]. For the other three wavelengths, the increase of pH causes a higher UV absorbance of the aqueous chlorine (Figure 2-7).
(3) The quantum yield of HOCl is higher than that of OCl^-, resulting in a lower •OH formation at alkaline pH [49].

(4) Both HOCl and OCl^- react with •OH (R8, 9 in Table 2-1) and •Cl (R11, 12), however the OCl^- is more reactive towards the two radicals ($k_9 > k_8$: $k_8=8.5\times10^4$~2.0×10^9 $M^{-1}s^{-1}$, $k_9=8.8\times10^8$~9.8×10^9 $M^{-1}s^{-1}$; $k_{12} > k_{11}$: $k_{11}=3\times10^9$ $M^{-1}s^{-1}$, $k_{12}=8.2\times10^9$ $M^{-1}s^{-1}$), meaning that the radical scavenging effect of OCl^- might be stronger than that of HOCl. On the other hand, all these four reactions generate ClO• which may also contribute to the degradation of TMP. So, there might be a trade-off between the generation of •OH/Cl• and ClO•.

(5) The speciation of TMP/TMP^+ may not have significant effect on the reactivity of •OH towards TMP [5].

(6) According to Wu et al. [5], reactive chlorine species (RCS) contributed to 67.4%, 65.7% and 86.9% of the TMP degradation in the UV/chlorine process at pH 6.1, pH 7.1 and pH 8.8 respectively, which were higher than chlorine and •OH. Among the RCS, ClO• was reported to account for the most of degradation of TMT and its contribution increased with increasing pH; while Cl• was expected to play a vital role in the degradation of DAMP and its contribution decreased with pH because of its decreasing concentration [72].

Based on above, for the wavelength of 254 nm in this study, due to the limited absorbance of OCl^-, the increasing contribution of ClO• might not compensate for the declining concentration of Cl• and •OH as pH was adjusted from acidic to alkaline; while at 265, 275 and 310 nm, the increases of ClO• concentration might well offset the decrease of •OH and Cl• with increasing pH. Besides, the relative increment of k_f' values for 310 nm (~10 times from pH 6 to pH 9) was much higher than that of 265 nm and 275 nm (~5 times), suggesting that the pH dependency of UV/chlorine process might become larger at higher wavelength. This phenomenon was also supported by Yin et al.[56].

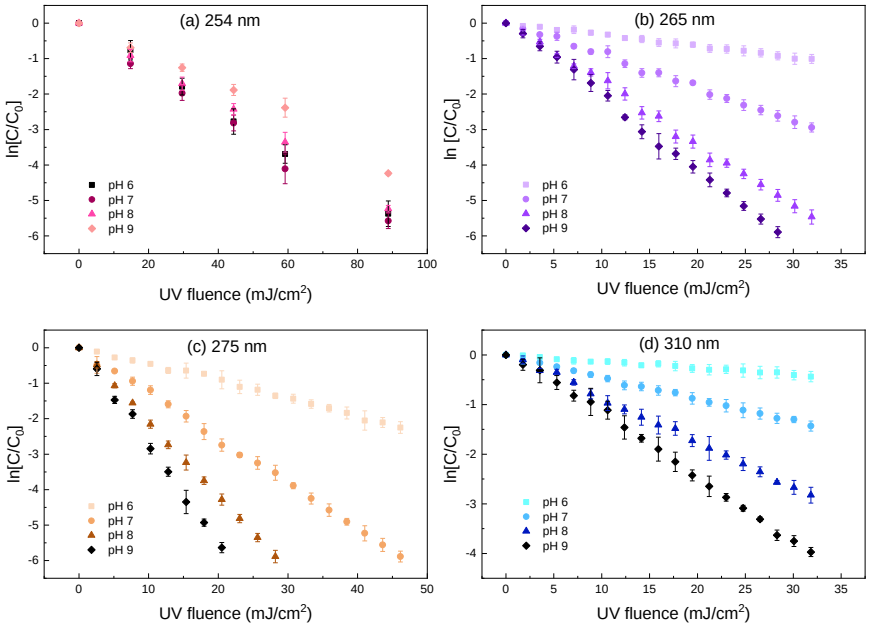

Figure 4-5: TMP degradation by UV/chlorine process as a function of UV fluence at various pHs and wavelengths. Condition: $[TMP]_0$=200 µg/L, $[chlorine]_0$= 3 mg/L as Cl_2.

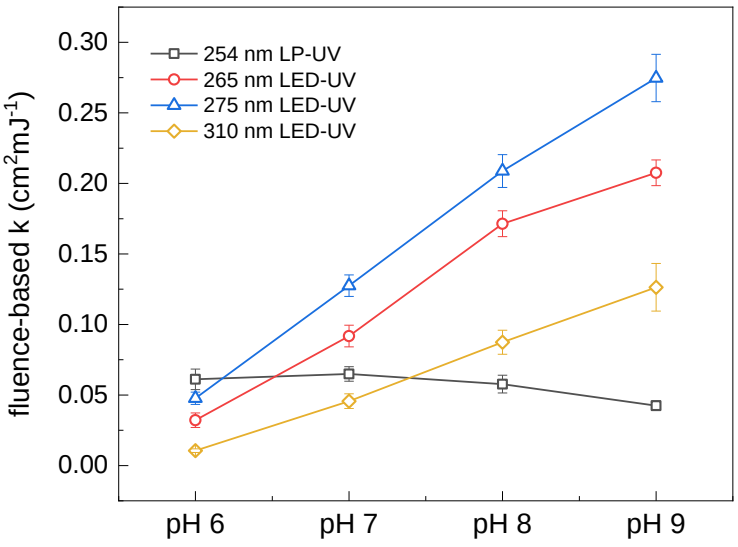

Figure 4-6: Fluence-based pseudo-first-order rate constants of TMP degradation by UV/chlorine at various pHs and wavelengths. Condition: $[TMP]_0$=200 µg/L, $[chlorine]_0$= 3 mg/L as Cl_2.

4.1.4 Effect of chlorine dosage

The increase of chlorine dosage could enhance the degradation of TMP. Take 275 nm as an example (Figure 4-7), the TMP removal by UV/chlorine increased from 36% to >99% at the UV fluence of 46 mW/cm^2 when the chlorine dosage increased from 0.3 mg/L to 1 mg/L; while the elimination of TMP (>99% removal) could be obtained at even lower UV fluence with higher chlorine dosage (22 mW/cm^2 for 3 mg/L Cl_2 and 16 mW/cm^2 for 6 mg/L Cl_2). In Figure

4-8, the fluence-based rate constants with various chlorine dosage were compared for the three LED-UV systems. The k_f' values in the three systems all exhibited almost linear relationships with chlorine dosage when [chlorine]$_0$ was lower than 3 mg/L. The k_f' increased by 49, 25 and 12 times as [chlorine]$_0$ increased from 0.3 to 3 mg/L, at the wavelength of 265 nm, 275 nm and 310 nm, respectively. However, the three wavelengths behaved differently as chlorine dosage increased further: for 265 nm, k_f' seemed to reach a plateau when [chlorine]$_0$ was larger than 3 mg/L; for 275 nm, k_f' continued increasing but with a slower rate; for 310 nm, k_f' increased more rapidly as chlorine changed from 3 mg/L to 6 mg/L.

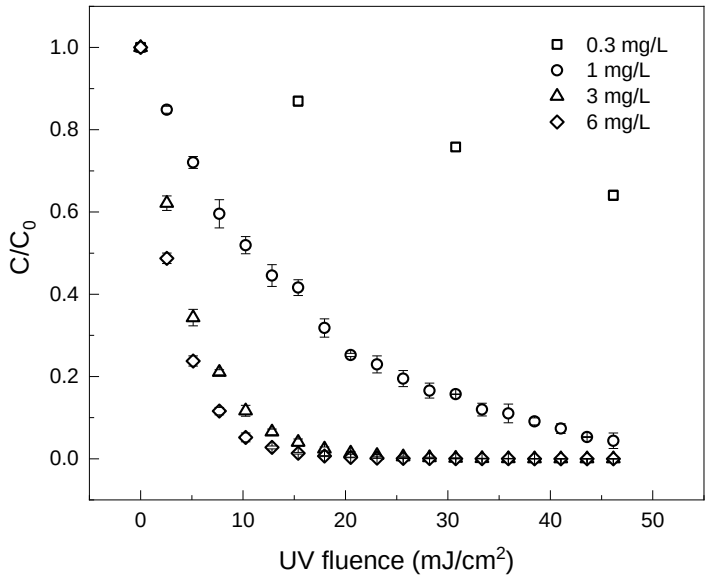

Figure 4-7: TMP degradation by 275 nm-UV/chlorine process with various chlorine dosage. Condition: [TMP]$_0$=200 µg/L, pH 8.

The addition of chlorine promoted the TMP degradation by enhancing the direct reaction of HOCl/OCl^- with the target pollutant and by generating more reactive radicals as well. The linear relationship between the pollutant degradation and the chlorine dose has also been observed in previous studies both in dark chlorination and UV/chlorine process [5], [49]. Some researchers attributed this linear relation to the reaction of ClO• with TMP whose yield increased with increasing chlorine dosage [5]. The radical scavenging rate of HOCl and OCl^- might also increase as the chlorine dosage increases (R8,9,11,12 in Table 2-1). At a certain dosage, the radical scavenging effect might overweigh the radical generation, leading to a lower or even negative increasing rate of pollutant decomposition [59]. This might explain the variation of k_f' at [chlorine]$_0$ of 3~6 mg/L in this study. Moreover, 265 nm system appeared to be the most sensitive to the chlorine dosage amongst the three LED-UV systems, which is likely due to the higher quantum yield of HOCl/OCl^- at this wavelength. The surge of k_f' at chlorine dosage of

6 mg/L in the 310 nm-system might also relate to the generation of $O(^1D)$, $O(^3P)$ and O_3 in the system [49].

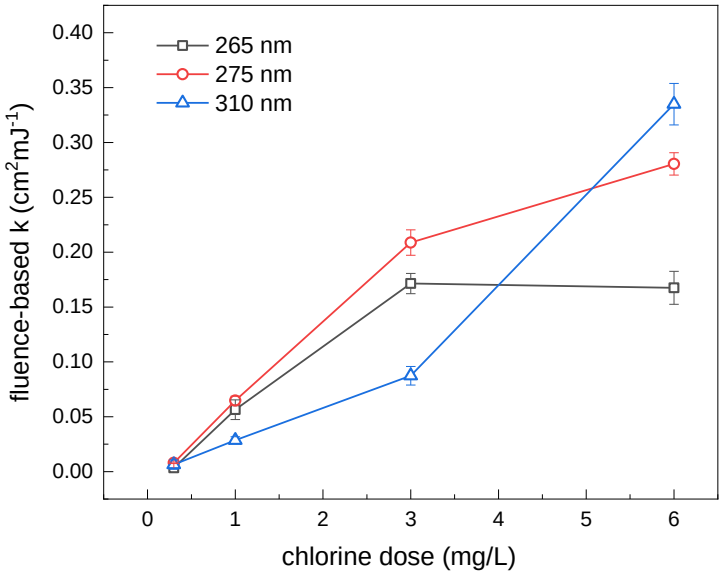

Figure 4-8: Fluence-based pseudo-first-order rate constants of TMP degradation by UV/chlorine with various chlorine dosage. Condition: $[TMP]_0$=200 µg/L, pH 8.

4.1.5 Effect of NOM (humic acid)

The effect of humic acid (HA, one major component of NOM) on TMP degradation by UV/chlorine process was examined. The total organic carbon (TOC) levels of HA solutions were measured and listed in Table 4-1. The presence of HA hindered the removal of TMP during UV/chlorine process, and the inhibitory effect became stronger as the concentration of HA increased from 5 mg/L to 20 mg/L. The fluence-based rate constant $k'_{f,w/o\ HA}$ of TMP degradation without the addition of HA were determined as 0.17, 0.21 and 0.09 cm^2mJ^{-1}, respectively for 265 nm, 275 nm and 310 nm system. When the HA level increased to 20 mg/L, the $k'_{f,w/\ HA}$ values for the three systems decreased to a similar level i.e. around 0.02 cm^2mJ^{-1}, with reductions of 85.90%, 88.51% and 73.41%, respectively. The reduction of k'_f was relatively higher in 265nm- and 275nm-system, compared to 310nm-system.

The inhibitory effect of HA was also observed for the removal of other micropollutants by UV/chlorine process, such as diuron [81] and carbamazepine [49]. HA can not only compete with the target micropollutant for UV light but also scavenge the reactive oxidant species (ROS) generated in the system [82]. The absorption coefficient of HA was found to decrease with increasing wavelength in the UV range. The degradation of HA itself during UV/chlorine was investigated recently by Gao et al.[74]. Their results revealed that the reactions with ROS

contributed much more to the HA degradation than chlorination and direct UV photolysis. More notably, the degradation rate of HA was observed to be faster at the wavelength of 275 nm than 310 nm due to the synergistic effect of absorptivity and quantum yields of HOCl/OCl^-. This might explain the more remarkable inhibitory effect of HA on TMP removal at 275 nm and 265 nm in this study.

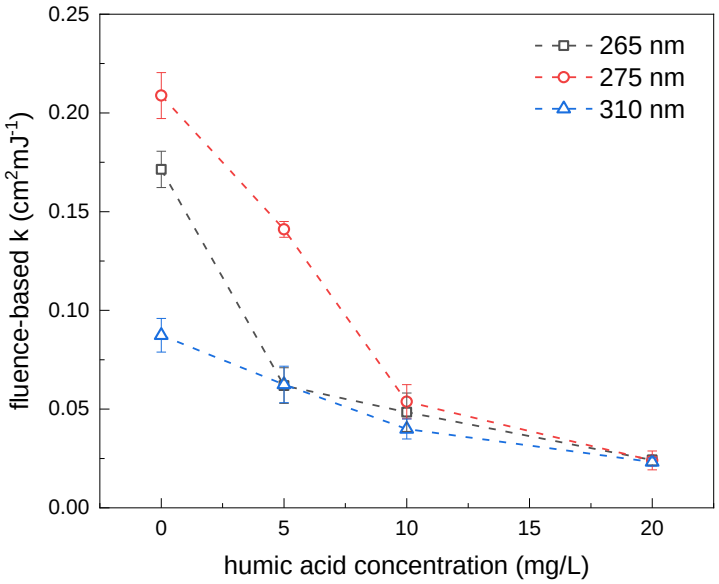

Figure 4-9: Fluence-based pseudo-first-order rate constants of TMP degradation by UV/chlorine with various concentrations of humic acid. Condition: $[TMP]_0$=200 μg/L, $[chlorine]_0$=3 mg/L as Cl_2, pH 8.

Table 4-1: TOC level of HA solution and the effect of HA on TMP degradation. Condition: same as Figure 4-9.

Humic acid concentration (mg/L)	TOC (mg C/L)	Reduction of degradation rate $\frac{k'_{f,w/o\ HA}-k'_{f,w/\ HA}}{k'_{f,w/o\ HA}}$ (%)		
		265 nm	275 nm	310 nm
5	0.881	63.87	32.45	28.49
10	1.469	71.74	74.25	54.31
20	2.635	85.90	88.51	73.41

4.2 Degradation products

The main degradation products of TMP detected during the 275 nm LED-UV/chlorine treatment were compounds with m/z of 325, 341, 307, 309, 445, 413, and 327 (Table 4-2). The formation of m/z 325 was likely due to the one chlorine substitution on TMP caused by the

oxidation of RCS and HOCl/OCl$^-$; while the detection of m/z 307 might be linked with the addition of -OH group through hydroxylation [5]. During the TMP degradation (TMP reduced by ~92%), the detected maximum intensities of m/z 325 by LC-MS/MS were about 2.5 times as high as those of m/z 307 (Figure 7-16), which might suggest that the contribution of •OH was less important than that of RCS and direct oxidation by HOCl/OCl$^-$. The formation of other compounds listed in Table 4-2 could be resulted from the combined effect of hydroxylation and chlorine substitution, and probably other more complex reactions such as demethylation and ring opening [5]. The compounds with m/z of 274 and 309 were not detected in previous studies where TMP was degraded by 254nm-UV/chlorine [5] or chlorination [78] or chlorine dioxide [83]. In addition, amongst the four major OBPs found in Wu et al.'s experiments [5], chloral hydrate ($C_2H_3O_2Cl_3$, m/z = 165) was detected in this work at higher concentrations relative to the other three OBPs – which were near undetectable levels. (Figure 4-10)

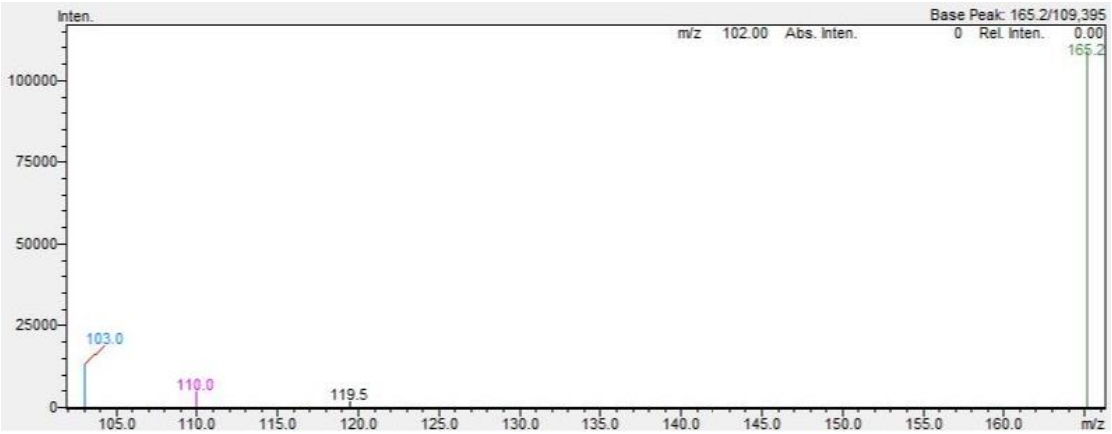

Figure 4-10: OBPs obtained during 275nm-LED-UV/chlorine process at 10 min

Thus, it was speculated that the wavelength applied in UV/chlorine process might influence the types of degradation products of TMP. Further, with the application of 275nm-LED-UV/chlorine process generated a smaller spectrum of halogenated daughter products compared to conventional 254nm-UV/chlorine. However, further analysis by advanced technology is really needed to verify this speculation. Table 4-2 below lists each degradation product identified in the application of 275nm- LED-UV/chlorine process, alongside with the proposed chemical formula arranged in incremental m/z ratios.

Table 4-2: Degradation products of TMP by UV/chlorine detected by LC-MS/MS ($[TMP]_0$=10mg/L, $[chlorine]_0$=15 mg/L, UV wavelength=275 nm, pH 8)

Compound	**Retention time (min)**	**$[M+H]^+$ (m/z)**	**Proposed chemical formula**
M-126	1.10	**165.2**	$C_2H_3O_2Cl_3$
M-112	1.13	**179**	$C_4H_5N_4Cl$
M-108	1.13	**183.1**	$C_{10}H_{15}O_3$
M-74	7.67	**217.1**	$C_{10}H_{14}O_3Cl$
M-17	6.83	**274.4**	$C_8H_{10}N_7Cl_2$ (from DAMP)
TMP (M)	1.67	**291.1**	$C_{14}H_{19}N_4O_3$
M+16	1.10	**307.1**	$C_{14}H_{19}N_4O_4$
M+18	8.70	**309.3**	$C_{14}H_{21}N_4O_4$
M+34	0.87	**325.1**	$C_{14}H_{18}N_4O_3Cl$
M+36	7.67	**326.5**	$C_{13}H_{16}N_4O_4Cl$
M+50	8.78	**341.4**	$C_{14}H_{18}N_4O_4Cl$
M+52	1.68	**343.1**	$C_{14}H_{20}N_4O_4Cl$
M+100	8.95	**391.4**	$C_{14}H_{17}N_4O_5Cl_2$
M+140	9.08	**413**	$C_{14}H_{20}N_4O_4Cl_3$
M+154	8.95	**445.4**	$C_{14}H_{17}N_4O_4Cl_4$

5 Conclusions and Recommendations

5.1 Conclusions

UV/chlorine AOP was proved to be more effective in degrading TMP than dark chlorination and direct UV photolysis. Higher degradation rate constants of TMP during UV/chlorine process were obtained at alkaline pH by using LED-UV at wavelengths of 265 nm, 275 nm and 310 nm, as compared to acidic pH. The UV wavelength at 275 nm was the most suitable one for TMP removal at pH 7 to 9 among the four tested wavelengths. Besides, the degradation rate of TMP increased almost linearly with the increasing chlorine dosage within the range of 0.3-3 mg/L. The presence of humic acid in water hindered the TMP degradation. The preliminary analysis of intermediates suggested that TMP could not be largely mineralized by UV/chlorine process with a UV dosage less than 600 mJ/cm^2. On the contrary, a number of compounds with higher molecular weight were generated during the treatment. Plausibly, the permutation of UV wavelength might affect the types of degradation products of TMP due to the contribution of radical species involved at each wavelength.

Based on this study, UV/chlorine process could achieve a good performance on TMP removal at alkaline pHs. Although this result was observed for one compound, it could have wider implications for other micropollutants sharing similar functional groups with TMP. Moreover, this work provides some references for the optimization of UV wavelength in the UV/chlorine AOP.

5.2 Recommendations

5.2.1 Experimental improvement

Due to the limitation of time, there were still some experimental gaps, which could be circumvented or improved in the following ways:

- A proper collimating tube should be applied for the LED-UV devices, so that the average UV fluence rate could be easily measured by a radiometer;
- The gradient program of LC-MS/MS should be further optimized to avoid overlapping of the individual peaks of TMP degradation products on the spectrum;
- A lower and more environmental-relevant TMP concentration should be used as the initial level to better simulate the TMP removal in real-world applications.
- Experiments on real water samples are desired.

5.2.2 Further research

- Based on the findings in section 4.1.5, various oxidation products are generated during TMP degradation by LED-UV/chlorine, including chloro-substituted compounds. Wang et al. reported that the absorbable organic chlorine (AOCl) level in the carbamazepine solution treated by LED-UV/chlorine was higher than that treated by chlorination [49]. Therefore, the formation of chloro-substituted oxidation by-products should be emphasized in the LED-UV/chlorine treatment. The toxicity evaluation should be conducted in further investigation.
- The TMP oxidation products were only preliminarily analyzed by proposing the chemical formulae in this project. The structure of each product is recommended to be studied in future study. Besides, the change of abundance of each product with time need to be investigated because it would be useful for determining the proper UV fluence and building the degradation pathways. Moreover, the effect of wavelength and pH on the types of oxidation products should be further verified.
- The research about roles of various ROS during the decomposition of TMP by LED-UV/chlorine process is helpful for the better understanding of the degradation mechanism, which is also recommended.
- The compact design of LED-UV provides the possibility of the polychromatic emissions at selected wavelengths in one UV reactor. So, the performance of combined-emission-UV/chlorine (e.g. 275/265 nm) on the treatment of TMP or other organic micropollutants could be examined in the future.

6 Bibliography

[1] Y. Yang, Y. S. Ok, K.-H. Kim, E. E. Kwon, and Y. F. Tsang, "Occurrences and removal of pharmaceuticals and personal care products (PPCPs) in drinking water and water/sewage treatment plants: A review," *Science of the Total Environment*, vol. 596, pp. 303–320, 2017.

[2] A. J. Ebele, M. A.-E. Abdallah, and S. Harrad, "Pharmaceuticals and personal care products (PPCPs) in the freshwater aquatic environment," *Emerging Contaminants*, vol. 3, no. 1, pp. 1–16, 2017.

[3] Q. Sui, X. Cao, S. Lu, W. Zhao, Z. Qiu, and G. Yu, "Occurrence, sources and fate of pharmaceuticals and personal care products in the groundwater: a review," *Emerging Contaminants*, vol. 1, no. 1, pp. 14–24, 2015.

[4] L. P. Padhye, H. Yao, F. T. Kung'u, and C.-H. Huang, "Year-long evaluation on the occurrence and fate of pharmaceuticals, personal care products, and endocrine disrupting chemicals in an urban drinking water treatment plant," *Water Research*, vol. 51, pp. 266–276, Mar. 2014.

[5] Z. Wu, J. Fang, Y. Xiang, C. Shang, X. Li, F. Meng and X. Yang, "Roles of reactive chlorine species in trimethoprim degradation in the UV/chlorine process: Kinetics and transformation pathways," *Water Research*, vol. 104, pp. 272–282, Nov. 2016.

[6] M. Y. Haller, S. R. Müller, C. S. McArdell, A. C. Alder, and M. J.-F. Suter, "Quantification of veterinary antibiotics (sulfonamides and trimethoprim) in animal manure by liquid chromatography–mass spectrometry," *Journal of Chromatography A*, vol. 952, no. 1–2, pp. 111–120, 2002.

[7] B. Kolar, L. Arnuš, B. Jeretin, A. Gutmaher, D. Drobne, and M. K. Durjava, "The toxic effect of oxytetracycline and trimethoprim in the aquatic environment," *Chemosphere*, vol. 115, pp. 75–80, 2014.

[8] "NITE - Chemical Management Field - GHS Information." [Online]. Available: http://www.safe.nite.go.jp/english/ghs/17-mhlw-0016e.html. [Accessed: 10-Feb-2019].

[9] K. S. Jewell, S. Castronovo, A. Wick, P. Falås, A. Joss, and T. A. Ternes, "New insights into the transformation of trimethoprim during biological wastewater treatment," *Water Research*, vol. 88, pp. 550–557, Jan. 2016.

[10] D. Wang, Q. Sui, S. Lu, W. Zhao, Z. Qiu, Z. Miao and G. Yu, "Occurrence and Removal of Six Pharmaceuticals and Personal Care Products in a Wastewater Treatment Plant Employing Anaerobic/Anoxic/Aerobic and Uv Processes in Shanghai, China," *Environmental Science and Pollution Research*, vol. 21, no. 6, pp. 4276–4285, 2014.

[11] N. Le-Minh, S. J. Khan, J. E. Drewes, and R. M. Stuetz, "Fate of antibiotics during municipal water recycling treatment processes," *Water Research*, vol. 44, no. 15, pp. 4295–4323, Aug. 2010.

[12] A. Göbel, C. S. McArdell, A. Joss, H. Siegrist, and W. Giger, "Fate of sulfonamides, macrolides, and trimethoprim in different wastewater treatment technologies," *Science of The Total Environment*, vol. 372, no. 2, pp. 361–371, Jan. 2007.

[13] M. R. Boleda, M. T. Galceran, and F. Ventura, "Behavior of pharmaceuticals and drugs of abuse in a drinking water treatment plant (DWTP) using combined conventional and ultrafiltration and reverse osmosis (UF/RO) treatments," *Environmental pollution*, vol. 159, no. 6, pp. 1584–1591, 2011.

[14] "Membrane Filtration - Advantages and Disadvantages." [Online]. Available: http://www.separationprocesses.com/Membrane/MT_Chp05f.htm. [Accessed: 25-Mar-2019].

[15] "Water Treatability Database." [Online]. Available: https://iaspub.epa.gov/tdb/pages/treatment/treatmentOverview.do?treatmentProcessId=2074826383. [Accessed: 25-Mar-2019].

[16] L. Rizzo, S. Malato, D. Antakyali, V. Beretsou, M. Dolic, W. Gernjak, E. Heath, I.

Ivancev-Tumbas, P. Karaolia, A. Lado Ribeiro, G. Mascolo, C. McArdell, H. Schaar, A. Silva and D. Fatta-Kassinos, "Consolidated vs new advanced treatment methods for the removal of contaminants of emerging concern from urban wastewater," *Science of The Total Environment*, vol. 655, pp. 986–1008, Mar. 2019.

[17] K. D. Brown, J. Kulis, B. Thomson, T. H. Chapman, and D. B. Mawhinney, "Occurrence of antibiotics in hospital, residential, and dairy effluent, municipal wastewater, and the Rio Grande in New Mexico," *Science of The Total Environment*, vol. 366, no. 2, pp. 772–783, Aug. 2006.

[18] A. J. Watkinson, E. J. Murby, D. W. Kolpin, and S. D. Costanzo, "The occurrence of antibiotics in an urban watershed: from wastewater to drinking water," *Science of the total environment*, vol. 407, no. 8, pp. 2711–2723, 2009.

[19] A. J. Watkinson, E. J. Murby, and S. D. Costanzo, "Removal of antibiotics in conventional and advanced wastewater treatment: Implications for environmental discharge and wastewater recycling," *Water Research*, vol. 41, no. 18, pp. 4164–4176, Oct. 2007.

[20] P. H. Roberts and K. V. Thomas, "The occurrence of selected pharmaceuticals in wastewater effluent and surface waters of the lower Tyne catchment," *Science of the Total Environment*, vol. 356, no. 1–3, pp. 143–153, 2006.

[21] T.-H. Le, C. Ng, N. H. Tran, H. Chen, and K. Y.-H. Gin, "Removal of antibiotic residues, antibiotic resistant bacteria and antibiotic resistance genes in municipal wastewater by membrane bioreactor systems," *Water Research*, vol. 145, pp. 498–508, Nov. 2018.

[22] J. Margot, C. Kienle, A. Magnet, M.Weil, L. Rossi, L. de Alencastro, C. Abegglen, D. Thonney, N. Chèvre, M. Schärer and D. Barry, "Treatment of micropollutants in municipal wastewater: Ozone or powdered activated carbon?," *Science of The Total Environment*, vol. 461–462, pp. 480–498, Sep. 2013.

[23] A. Göbel, A. Thomsen, C. S. McArdell, A. Joss, and W. Giger, "Occurrence and sorption behavior of sulfonamides, macrolides, and trimethoprim in activated sludge treatment," *Environmental science & technology*, vol. 39, no. 11, pp. 3981–3989, 2005.

[24] R. Mailler, J. Gasperi, Y. Coquet, S. Deshayes, S. Zedek, C. Cren-Olivé, N. Cartiser, V. Eudes, A. Bressy, E. Caupos, R. Moilleron, G. Chebbo and V. Rocher, "Study of a large scale powdered activated carbon pilot: Removals of a wide range of emerging and priority micropollutants from wastewater treatment plant effluents," *Water Research*, vol. 72, pp. 315–330, Apr. 2015.

[25] K. G. Karthikeyan and M. T. Meyer, "Occurrence of antibiotics in wastewater treatment facilities in Wisconsin, USA," *Science of the Total Environment*, vol. 361, no. 1–3, pp. 196–207, 2006.

[26] X. Yang, R. C. Flowers, H. S. Weinberg, and P. C. Singer, "Occurrence and removal of pharmaceuticals and personal care products (PPCPs) in an advanced wastewater reclamation plant," *Water Research*, vol. 45, no. 16, pp. 5218–5228, Oct. 2011.

[27] S. Kleywegt, V. Pileggi, P. Yang, C. Hao, X. Zhao, C. Rocks, S. Trach, P. Cheung and B. Whitehead, "Pharmaceuticals, hormones and bisphenol A in untreated source and finished drinking water in Ontario, Canada—occurrence and treatment efficiency," *Science of the Total Environment*, vol. 409, no. 8, pp. 1481–1488, 2011.

[28] D. Kanakaraju, B. D. Glass, and M. Oelgemöller, "Advanced oxidation process-mediated removal of pharmaceuticals from water: A review," *Journal of environmental management*, vol. 219, pp. 189–207, 2018.

[29] D. B. Miklos, C. Remy, M. Jekel, K. G. Linden, J. E. Drewes, and U. Hübner, "Evaluation of advanced oxidation processes for water and wastewater treatment – A critical review," *Water Research*, vol. 139, pp. 118–131, Aug. 2018.

[30] J. C. Kruithof, P. C. Kamp, and B. J. Martijn, "UV/H2O2 treatment: a practical solution for organic contaminant control and primary disinfection," *Ozone: Science and Engineering*, vol. 29, no. 4, pp. 273–280, 2007.

[31] "Advanced Oxidation UV Peroxide - Spartan Environmental Technologies." [Online]. Available: https://www.spartanwatertreatment.com/advanced-oxidation-UV-

peroxide.html. [Accessed: 29-Mar-2019].
[32] E. Rosenfeldt, A. Boal, J. Springer, B. Stanford, S. Rivera, R. Kashinkunti and D. Metz, "Comparison of UV-mediated Advanced Oxidation," *Journal-American Water Works Association*, vol. 105, no. 7, pp. 29–33, 2013.
[33] M. A. Barakat, J. M. Tseng, and C. P. Huang, "Hydrogen peroxide-assisted photocatalytic oxidation of phenolic compounds," *Applied Catalysis B: Environmental*, vol. 59, no. 1–2, pp. 99–104, 2005.
[34] D. B. Miklos, C. Remy, M. Jekel, K. G. Linden, J. E. Drewes, and U. Hübner, "Evaluation of advanced oxidation processes for water and wastewater treatment–A critical review," *Water Research*, vol. 139, pp. 118–131, 2018.
[35] Y. Huang, Z. Nie, C. Wang, Y. Li, M. Xu, and R. Hofmann, "Quenching H 2 O 2 residuals after UV/H 2 O 2 oxidation using GAC in drinking water treatment," *Environmental Science: Water Research & Technology*, vol. 4, no. 10, pp. 1662–1670, 2018.
[36] G. Galjaard, B. Martijn, E. Koreman, M. Bogosh, and J. Malley, "Performance evaluation SIX®-Ceramac® in comparison with conventional pre-treatment techniques for Surface Water Treatment," *Water Practice and Technology*, vol. 6, no. 4, 2011.
[37] J. Fang, Y. Fu, and C. Shang, "The roles of reactive species in micropollutant degradation in the UV/free chlorine system," *Environmental science & technology*, vol. 48, no. 3, pp. 1859–1868, 2014.
[38] J. E. Forsyth, P. Zhou, Q. Mao, S. S. Asato, J. S. Meschke, and M. C. Dodd, "Enhanced inactivation of Bacillus subtilis spores during solar photolysis of free available chlorine," *Environmental science & technology*, vol. 47, no. 22, pp. 12976–12984, 2013.
[39] M. J. Watts and K. G. Linden, "Chlorine photolysis and subsequent OH radical production during UV treatment of chlorinated water," *Water Research*, vol. 41, no. 13, pp. 2871–2878, Jul. 2007.
[40] J. Jin, M. G. El-Din, and J. R. Bolton, "Assessment of the UV/chlorine process as an advanced oxidation process," *Water Research*, vol. 45, no. 4, pp. 1890–1896, 2011.
[41] C. Sichel, C. Garcia, and K. Andre, "Feasibility studies: UV/chlorine advanced oxidation treatment for the removal of emerging contaminants," *Water research*, vol. 45, no. 19, pp. 6371–6380, 2011.
[42] D. Wang, J. R. Bolton, and R. Hofmann, "Medium pressure UV combined with chlorine advanced oxidation for trichloroethylene destruction in a model water," *Water research*, vol. 46, no. 15, pp. 4677–4686, 2012.
[43] L. H. Nowell and J. Hoigné, "Photolysis of aqueous chlorine at sunlight and ultraviolet wavelengths—II. Hydroxyl radical production," *Water Research*, vol. 26, no. 5, pp. 599–605, 1992.
[44] P. Y. Chan, M. G. El-Din, and J. R. Bolton, "A solar-driven UV/Chlorine advanced oxidation process," *Water research*, vol. 46, no. 17, pp. 5672–5682, 2012.
[45] W. Ben, P. Sun, and C.-H. Huang, "Effects of combined UV and chlorine treatment on chloroform formation from triclosan," *Chemosphere*, vol. 150, pp. 715–722, 2016.
[46] C. K. Remucal and D. Manley, "Emerging investigators series: the efficacy of chlorine photolysis as an advanced oxidation process for drinking water treatment," *Environmental Science: Water Research & Technology*, vol. 2, no. 4, pp. 565–579, 2016.
[47] Y. Xiang, J. Fang, and C. Shang, "Kinetics and pathways of ibuprofen degradation by the UV/chlorine advanced oxidation process," *Water research*, vol. 90, pp. 301–308, 2016.
[48] C. Sichel, C. Garcia, and K. Andre, "Feasibility studies: UV/chlorine advanced oxidation treatment for the removal of emerging contaminants," *Water research*, vol. 45, no. 19, pp. 6371–6380, 2011.
[49] W. Wang, Q. Wu, Z. Li, Y. Lu, Y. Du, T. Wang, N. Huang and H. Hu, "Light-emitting diodes as an emerging UV source for UV/chlorine oxidation: carbamazepine degradation and toxicity changes," *Chemical Engineering Journal*, vol. 310, pp. 148–156, 2017.
[50] "City of Los Angeles Terminal Island Water Reclamation Plant selects innovative water reuse solution to address need for water security | Xylem US." [Online]. Available:

https://www.xylem.com/en-us/about-xylem/newsroom/press-releases/city-of-los-angeles-terminal-island-water-reclamation-plant-selects-innovative-water-reuse-solution-to-address-need-for-water-security2/. [Accessed: 30-Mar-2019].
[51] "A Water Treatment Alternative to Chlorine? | Engineering360." [Online]. Available: https://insights.globalspec.com/article/3112/a-water-treatment-alternative-to-chlorine. [Accessed: 30-Mar-2019].
[52] F. Rosario-Ortiz and V. Speight, "Can drinking water be delivered without disinfectants like chlorine and still be safe?," *The Conversation*. [Online]. Available: http://theconversation.com/can-drinking-water-be-delivered-without-disinfectants-like-chlorine-and-still-be-safe-55476. [Accessed: 30-Mar-2019].
[53] X. Yang, J. Sun, W. Fu, C. Shang, Y. Li, Y. Chen, W. Gan and J. Fang, "PPCP degradation by UV/chlorine treatment and its impact on DBP formation potential in real waters," *Water Research*, vol. 98, pp. 309–318, Jul. 2016.
[54] L. Qin, Y. Lin, B. Xu, C. Hu, F. Tian, T. Zhang, W. Zhu, H. Huang and N. Gao, "Kinetic models and pathways of ronidazole degradation by chlorination, UV irradiation and UV/chlorine processes," *Water research*, vol. 65, pp. 271–281, 2014.
[55] D. Wang, J. R. Bolton, S. A. Andrews, and R. Hofmann, "UV/chlorine control of drinking water taste and odour at pilot and full-scale," *Chemosphere*, vol. 136, pp. 239–244, Oct. 2015.
[56] R. Yin, L. Ling, and C. Shang, "Wavelength-dependent chlorine photolysis and subsequent radical production using UV-LEDs as light sources," *Water Research*, vol. 142, pp. 452–458, Oct. 2018.
[57] J. Chen, S. Loeb, and J.-H. Kim, "LED revolution: fundamentals and prospects for UV disinfection applications," *Environmental Science: Water Research & Technology*, vol. 3, no. 2, pp. 188–202, 2017.
[58] K. Song, M. Mohseni, and F. Taghipour, "Application of ultraviolet light-emitting diodes (UV-LEDs) for water disinfection: A review," *Water research*, vol. 94, pp. 341–349, 2016.
[59] M. Kwon, Y. Yoon, S. Kim, Y. Jung, T.-M. Hwang, and J.-W. Kang, "Removal of sulfamethoxazole, ibuprofen and nitrobenzene by UV and UV/chlorine processes: A comparative evaluation of 275 nm LED-UV and 254 nm LP-UV," *Science of the Total Environment*, vol. 637, pp. 1351–1357, 2018.
[60] B. F. Kalisvaart, "Re-use of wastewater: preventing the recovery of pathogens by using medium-pressure UV lamp technology," *Water Science and Technology; London*, vol. 50, no. 6, pp. 337–344, Sep. 2004.
[61] "Ultraviolet Systems." [Online]. Available: http://www.watertreatmentguide.com/ultraviolet_systems.htm. [Accessed: 15-Mar-2019].
[62] H. Bergmann, T. Iourtchouk, K. Schöps, and K. Bouzek, "New UV irradiation and direct electrolysis—promising methods for water disinfection," *Chemical Engineering Journal*, vol. 85, no. 2–3, pp. 111–117, 2002.
[63] "Medium Pressure & Low Pressure Lamps - Atlantium Technologies." [Online]. Available: https://www.atlantium.com/en/markets/aquaculture-eng/blog/medium-pressure-low-pressure-lamps.html. [Accessed: 06-Feb-2019].
[64] K. M. Johnson, M. A. Kumar, P. Ponmurugan, and B. M. Gananamangai, "Ultraviolet radiation and its germicidal effect in drinking water purification," *Journal of Phytology*, 2010.
[65] J. J. Jankowski, D. J. Kieber, K. Mopper, and P. J. Neale, "Development and Intercalibration of Ultraviolet Solar Actinometers," *Photochemistry and Photobiology*, vol. 71, no. 4, pp. 431–440, 2000.
[66] Bolton James R. and Linden Karl G., "Standardization of Methods for Fluence (UV Dose) Determination in Bench-Scale UV Experiments," *Journal of Environmental Engineering*, vol. 129, no. 3, pp. 209–215, Mar. 2003.

[67] H. J. Kuhn, S. E. Braslavsky, and R. Schmidt, “Chemical actinometry (IUPAC Technical Report),” *Pure and Applied Chemistry*, vol. 76, no. 12, pp. 2105–2146, 2004.
[68] J. R. Bolton, M. I. Stefan, P.-S. Shaw, and K. R. Lykke, “Determination of the quantum yields of the potassium ferrioxalate and potassium iodide–iodate actinometers and a method for the calibration of radiometer detectors,” *Journal of Photochemistry and Photobiology A: Chemistry*, vol. 222, no. 1, pp. 166–169, Jul. 2011.
[69] G. Matafonova and V. Batoev, “Recent advances in application of UV light-emitting diodes for degrading organic pollutants in water through advanced oxidation processes: A review,” *Water research*, vol. 132, pp. 177–189, 2018.
[70] M. A. Ibrahim, J. MacAdam, O. Autin, and B. Jefferson, “Evaluating the impact of LED bulb development on the economic viability of ultraviolet technology for disinfection,” *Environmental technology*, vol. 35, no. 4, pp. 400–406, 2014.
[71] L. H. Nowell and J. Hoigné, “Photolysis of aqueous chlorine at sunlight and ultraviolet wavelengths—I. Degradation rates,” *Water Research*, vol. 26, no. 5, pp. 593–598, May 1992.
[72] K. Guo, Z. Wu, C. Shang, B. Yao, S. Hou, X. Yang, W. Song and J. Fang, “Radical Chemistry and Structural Relationships of PPCP Degradation by UV/Chlorine Treatment in Simulated Drinking Water,” *Environ. Sci. Technol.*, vol. 51, no. 18, pp. 10431–10439, Sep. 2017.
[73] J. Fang, Y. Fu, and C. Shang, “The Roles of Reactive Species in Micropollutant Degradation in the UV/Free Chlorine System,” *Environ. Sci. Technol.*, vol. 48, no. 3, pp. 1859–1868, Feb. 2014.
[74] Z. Gao, Y. Lin, B. Xu, C. Yan, T. Zhang, T. Cao, W. Chu and N. Gao, “Effect of UV wavelength on humic acid degradation and disinfection by-product formation during the UV/chlorine process,” *Water Research*, 2019.
[75] Y. Feng, D. W. Smith, and J. R. Bolton, “Photolysis of aqueous free chlorine species (HOCl and OCl-) with 254 nm ultraviolet light,” *J. Environ. Eng. Sci.*, vol. 6, no. 3, pp. 277–284, May 2007.
[76] “phosphate buffer,” *Cold Spring Harb Protoc*, vol. 2006, no. 1, p. pdb.rec8543, Jun. 2006.
[77] S. Goldstein and J. Rabani, “The ferrioxalate and iodide–iodate actinometers in the UV region,” *Journal of Photochemistry and Photobiology A: Chemistry*, vol. 193, no. 1, pp. 50–55, 2008.
[78] M. C. Dodd and C. Huang, “Aqueous chlorination of the antibacterial agent trimethoprim: Reaction kinetics and pathways,” *Water Research*, vol. 41, no. 3, pp. 647–655, Feb. 2007.
[79] L. SI, “EFFECTS OF NATURAL ORGANIC MATTER ON PHOTOLYTIC AND PHOTOCATALYTIC DECOMPOSITION OF PHARMACEUTICALS,” PhD Thesis, 2016.
[80] C. Baeza and D. R. U. Knappe, “Transformation kinetics of biochemically active compounds in low-pressure UV Photolysis and UV/H2O2 advanced oxidation processes,” *Water Research*, vol. 45, no. 15, pp. 4531–4543, Oct. 2011.
[81] H. Xiang, Y. Shao, N. Gao, X. Lu, N. An, C. Tan and Z. Zheng, “Degradation of diuron by chlorination and UV/chlorine process: Degradation kinetics and the formation of disinfection by-products,” *Separation and Purification Technology*, vol. 202, pp. 365–372, 2018.
[82] S. Li and J. Hu, “Photolytic and photocatalytic degradation of tetracycline: effect of humic acid on degradation kinetics and mechanisms,” *Journal of hazardous materials*, vol. 318, pp. 134–144, 2016.
[83] P. Wang, Y. He, and C. Huang, “Oxidation of antibiotic agent trimethoprim by chlorine dioxide: reaction kinetics and pathways,” *Journal of Environmental Engineering*, vol. 138, no. 3, pp. 360–366, 2011.

7 Appendix

7.1 Ferrioxalate Actinometry

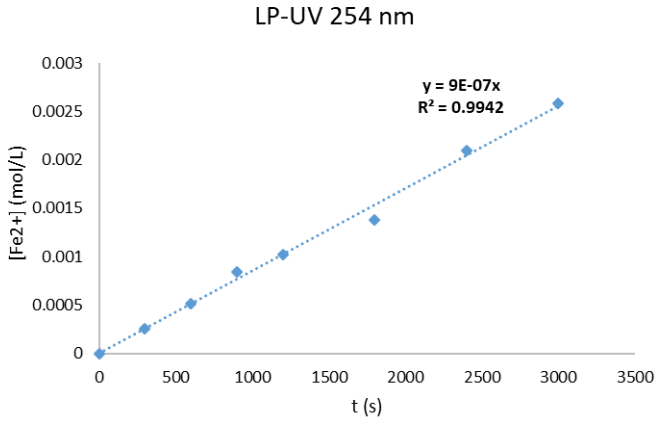

LP-UV 254 nm	value	unit
Slope	9.0×10^{-7}	$molL^{-1}s^{-1}$
UV absorbed (Equation 2-6)	6.45×10^{-7}	$EsL^{-1}s^{-1}$
Energy absorbed	0.3038	$JL^{-1}s^{-1}$ (mW/cm^3)
Average UV intensity (Equation 2-8)	0.2467	mW/cm^2

Figure 7-1: 254 nm LP-UV intensity measured by ferrioxalate actinometer

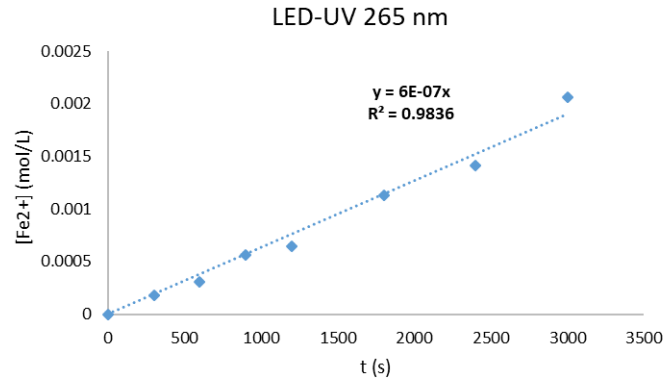

LED-UV 265 nm	value	unit
Slope	6.0×10^{-7}	$molL^{-1}s^{-1}$
UV absorbed (Equation 2-6)	4.84×10^{-7}	$EsL^{-1}s^{-1}$
Energy absorbed	0.2184	$JL^{-1}s^{-1}$ (mW/cm^3)
Average UV intensity (Equation 2-8)	0.1774	mW/cm^2

Figure 7-2: 265 nm LED-UV intensity measured by ferrioxalate actinometer

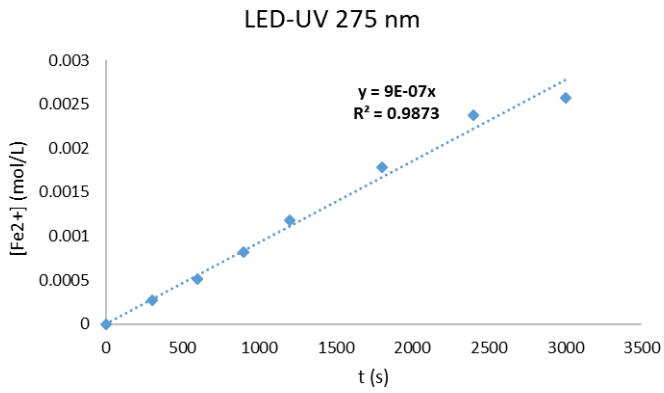

LED-UV 275 nm	value	unit
Slope	9.0×10^{-7}	$molL^{-1}s^{-1}$
UV absorbed (Equation 2-6)	7.26×10^{-7}	$EsL^{-1}s^{-1}$
Energy absorbed	0.3157	$JL^{-1}s^{-1}$ (mW/cm^3)
Average UV intensity (Equation 2-8)	0.2564	mW/cm^2

Figure 7-3: 275 nm LED-UV intensity measured by ferrioxalate actinometer

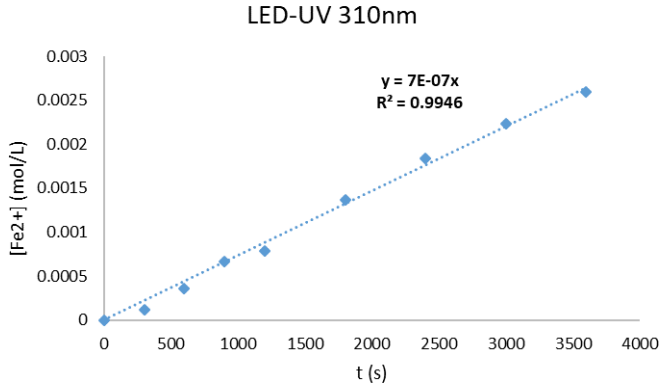

LED-UV 310 nm	value	unit
Slope	7.0×10^{-7}	$molL^{-1}s^{-1}$
UV absorbed (Equation 2-6)	5.65×10^{-7}	$EsL^{-1}s^{-1}$
Energy absorbed	0.2178	$JL^{-1}s^{-1}$ (mW/cm^3)
Average UV intensity (Equation 2-8)	0.1769	mW/cm^2

Figure 7-4: 310 nm LED-UV intensity measured by ferrioxalate actinometer

7.2 TMP degradation kinetics

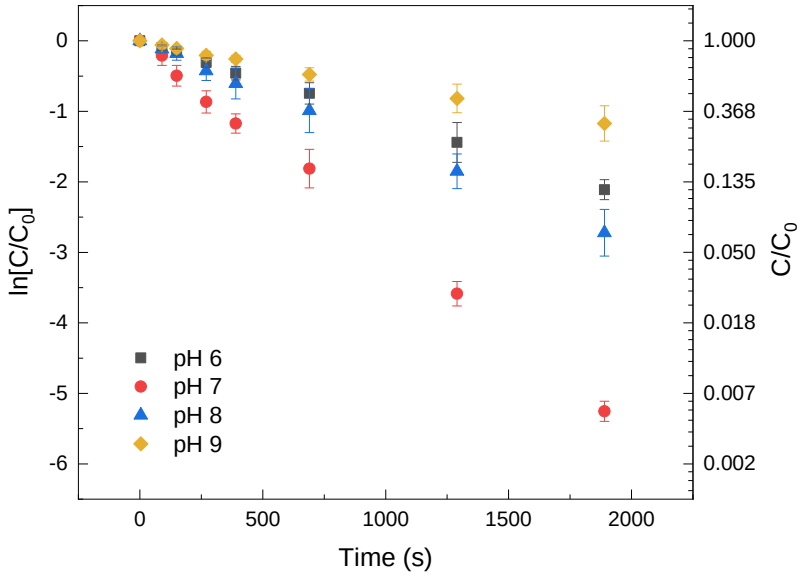

Figure 7-5: TMP degradation by dark chlorination at pH 6 – 9. Condition: $[TMP]_0$ = 200 µg/L, $[chlorine]_0$ =3 mg/L as Cl_2.

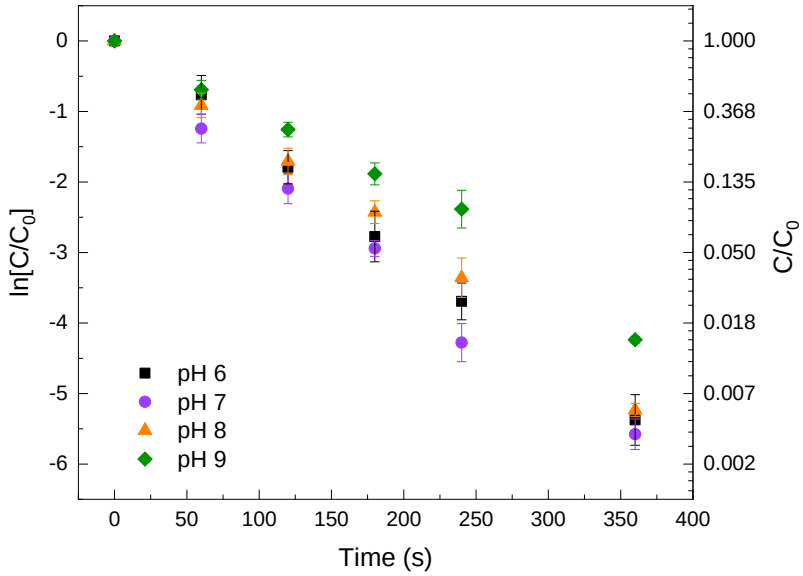

Figure 7-6: TMP degradation by LP-UV/chlorine (254 nm) at pH 6 – 9. Condition: $[TMP]_0$ = 200 µg/L, $[chlorine]_0$ =3 mg/L as Cl_2, UV intensity: 0.2467 mW/cm^2.

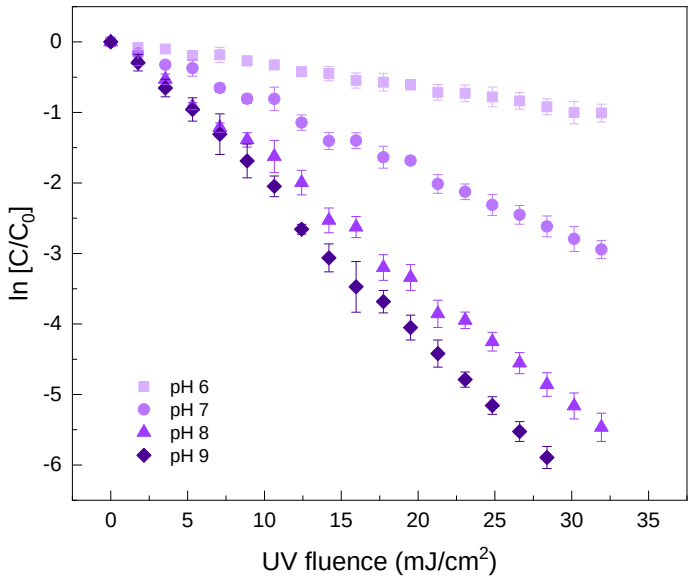

Figure 7-7: TMP degradation by 265 nm LED-UV/chlorine at pH 6 – 9. Condition: $[TMP]_0$ = 200 µg/L, $[chlorine]_0$ =3 mg/L as Cl_2, UV intensity: 0.1774 mW/cm^2.

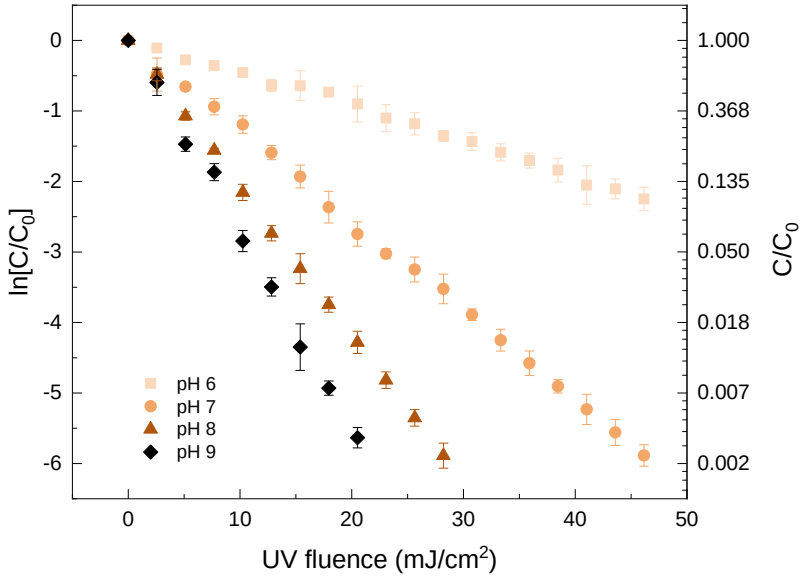

Figure 7-8: TMP degradation by 275 nm LED-UV/chlorine at pH 6 – 9. Condition: $[TMP]_0$ = 200 µg/L, $[chlorine]_0$ =3 mg/L as Cl_2, UV intensity: 0.2564 mW/cm^2.

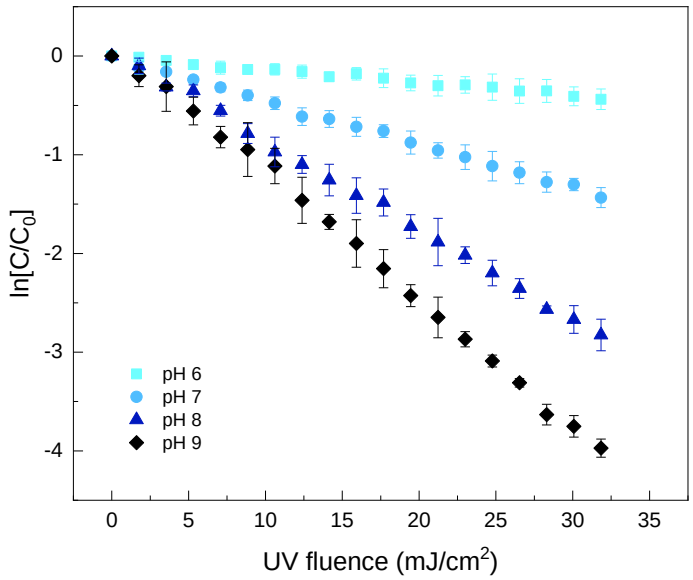

Figure 7-9: TMP degradation by 310 nm LED-UV/chlorine at pH 6 – 9. Condition: $[TMP]_0$ = 200 µg/L, $[chlorine]_0$ =3 mg/L as Cl_2, UV intensity: 0.1769 mW/cm^2.

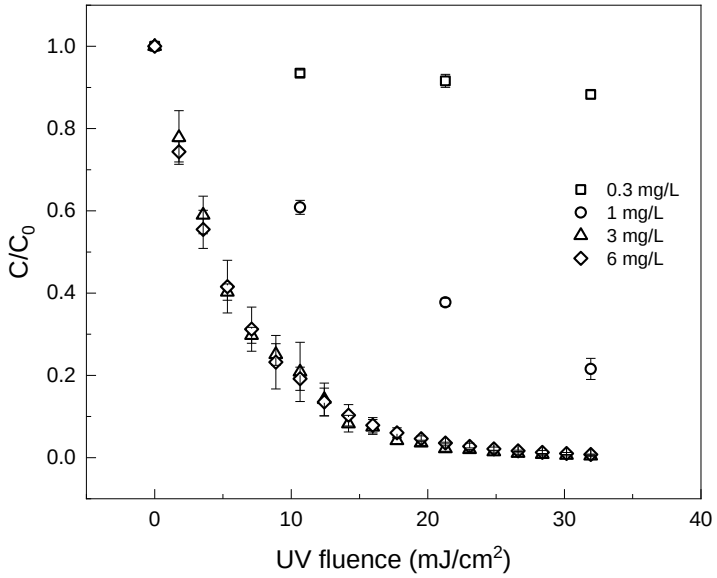

Figure 7-10: TMP degradation by 265 nm LED -UV/chlorine process with various chlorine dosage. Condition: $[TMP]_0$=200 µg/L, UV intensity: 0.1774 mW/cm^2, pH 8.

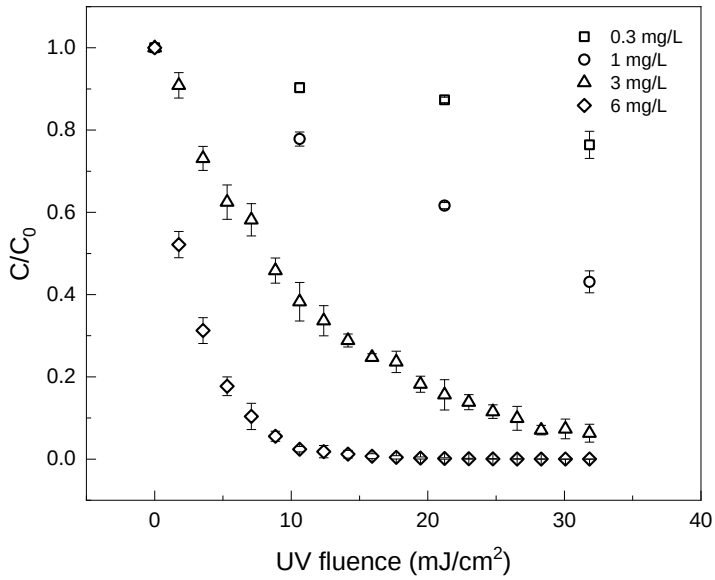

Figure 7-11: TMP degradation by 310 nm LED -UV/chlorine process with various chlorine dosage. Condition: $[TMP]_0$=200 µg/L, UV intensity: 0.1769 mW/cm^2, pH 8.

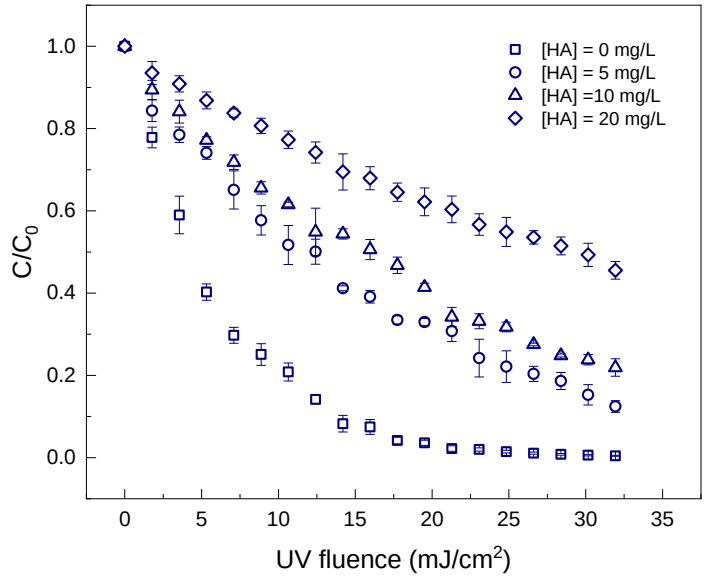

Figure 7-12: TMP degradation by 265 nm LED-UV/chlorine with various concentrations of humic acid. Condition: $[TMP]_0$=200 µg/L, $[chlorine]_0$=3 mg/L as Cl_2, UV intensity: 0.1774 mW/cm^2, pH 8.

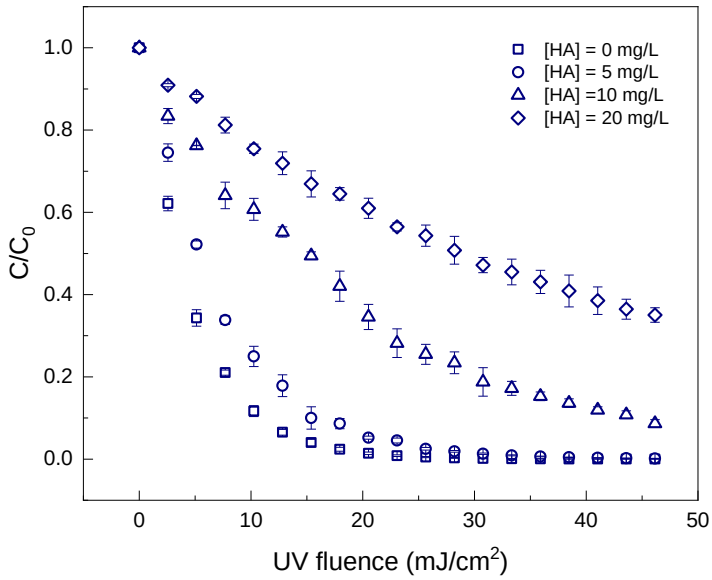

Figure 7-13: TMP degradation by 275 nm LED-UV/chlorine with various concentrations of humic acid. Condition: $[TMP]_0$=200 µg/L, $[chlorine]_0$=3 mg/L as Cl_2, UV intensity: 0.2564 mW/cm^2, pH 8.

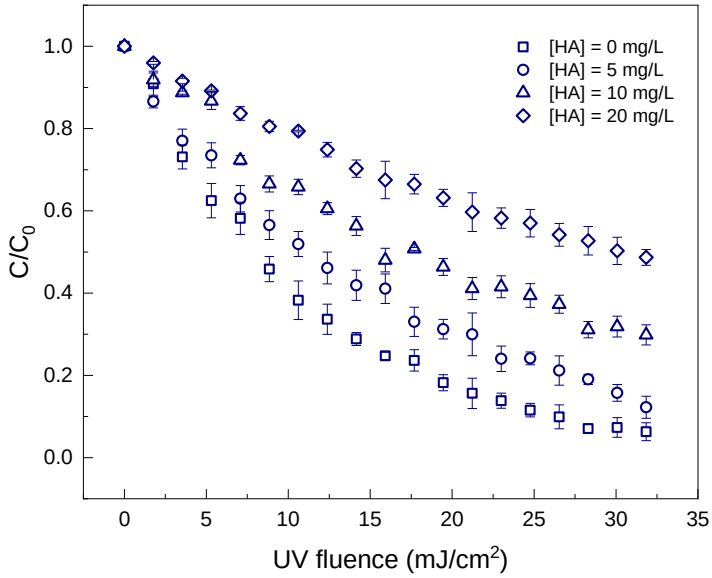

Figure 7-14: TMP degradation by 310 nm LED-UV/chlorine with various concentrations of humic acid. Condition: $[TMP]_0$=200 µg/L, $[chlorine]_0$=3 mg/L as Cl_2, UV intensity: 0.1769 mW/cm^2, pH 8.

7.3 TMP degradation products

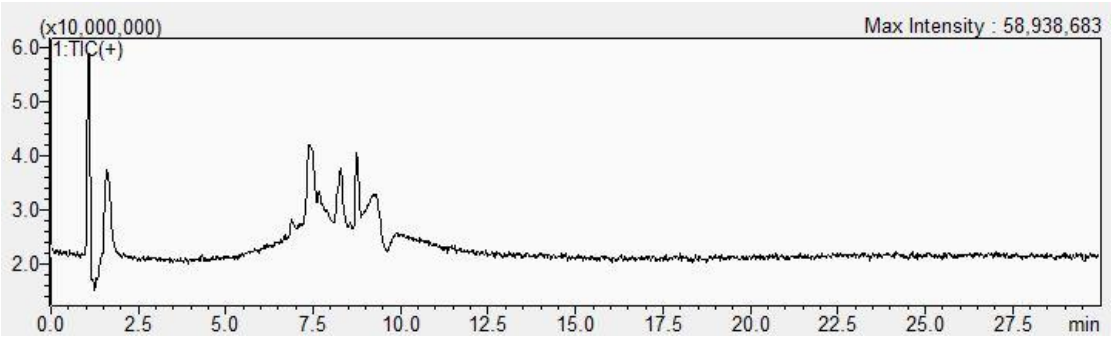

Figure 7-15: LC-MS/MS spectra of TMP degradation products: full scan. Condition: $[TMP]_0$ = 10 mg/L, $[chlorine]_0$ = 15 mg/L as Cl_2, UV fluence = 154 mJ/cm^2, wavelength =275 nm, pH 8.

a) m/z = 165

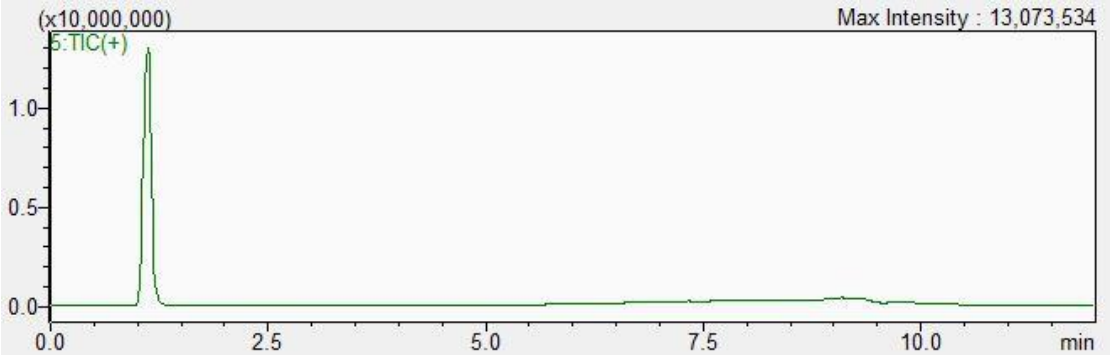

b) m/z = 179

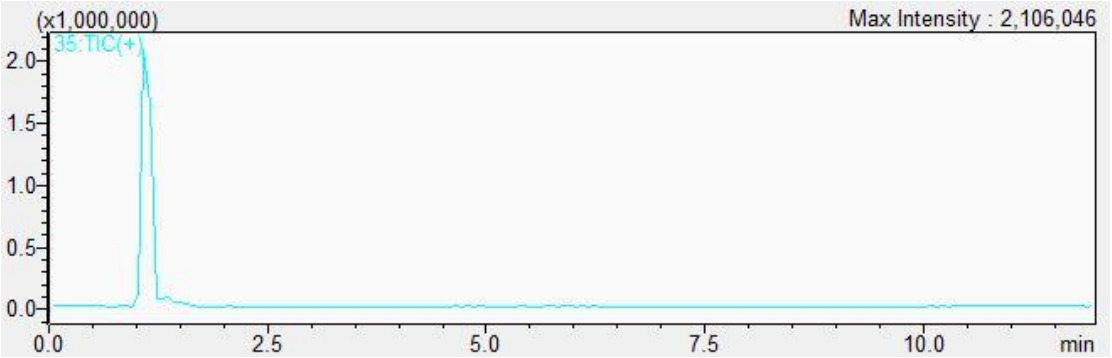

c) m/z = 183

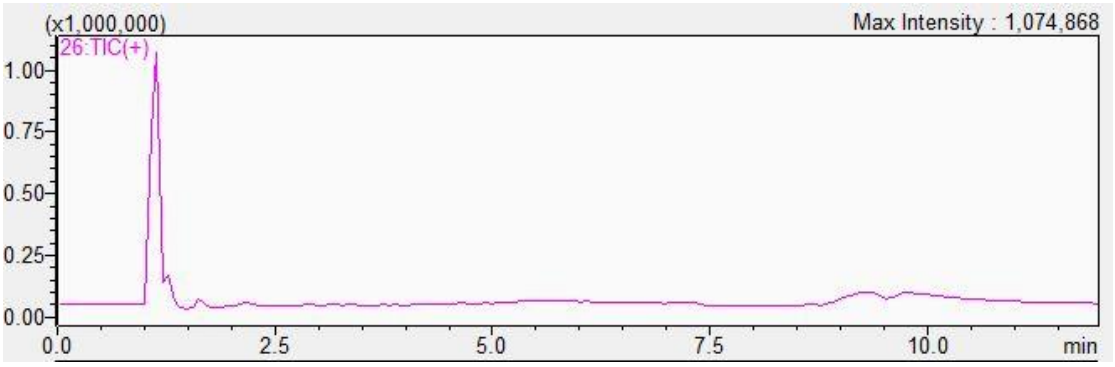

d) m/z = 271

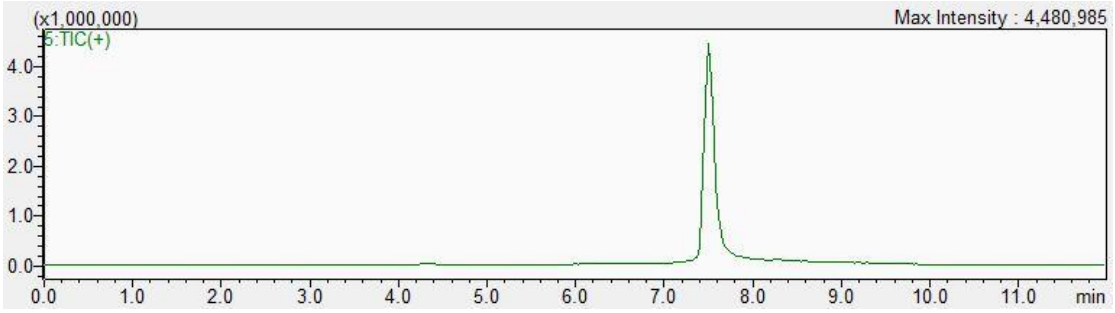

e) m/z = 274

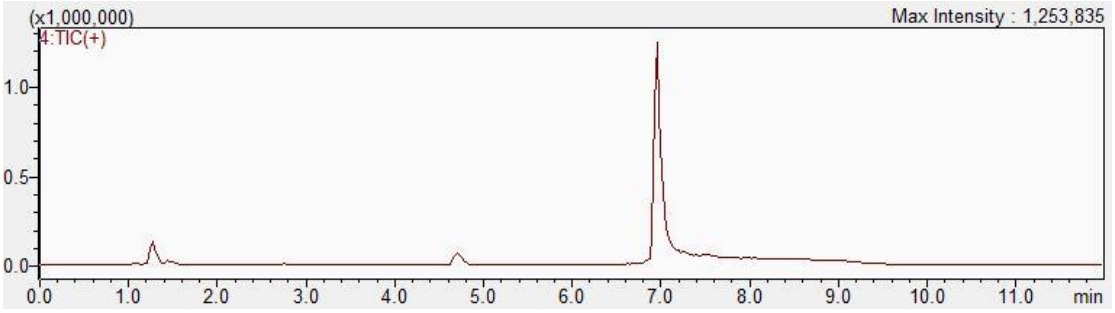

f) m/z = 291 (TMP)

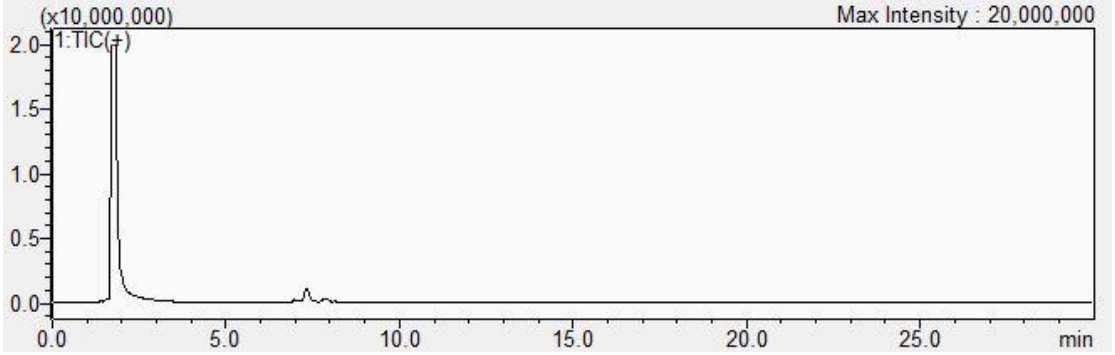

g) m/z = 307

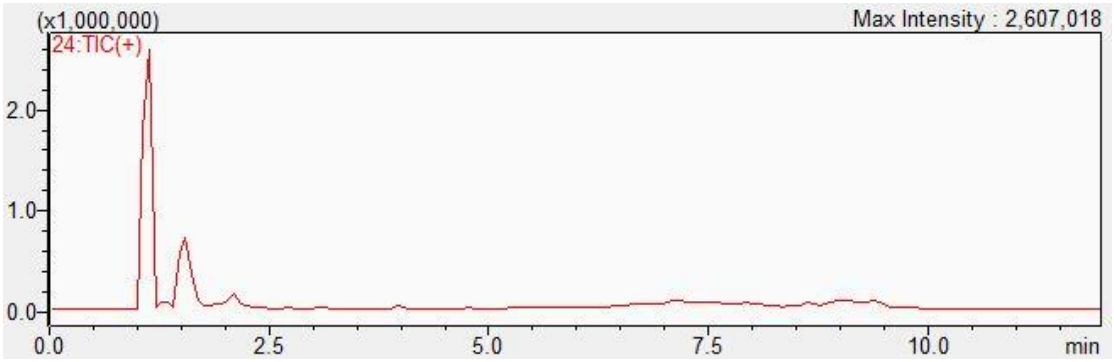

h) m/z = 309

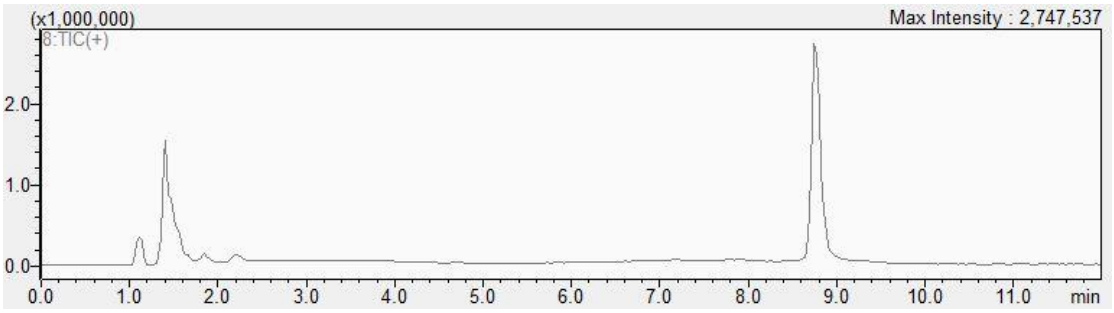

i) m/z = 325

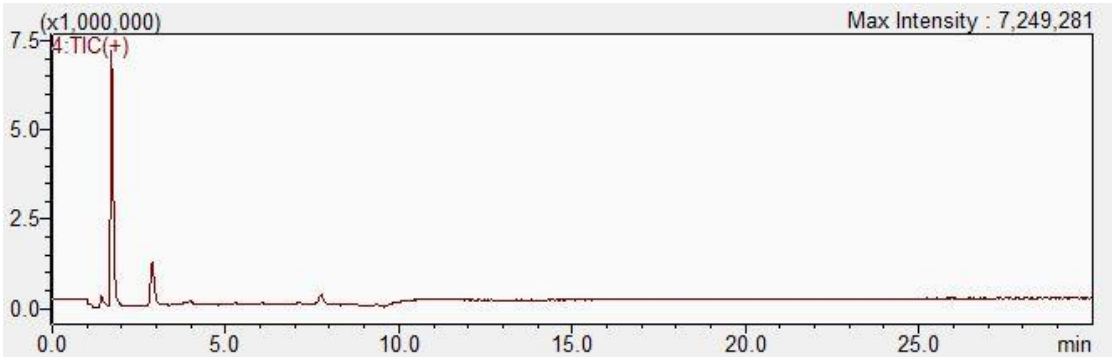

j) m/z = 327

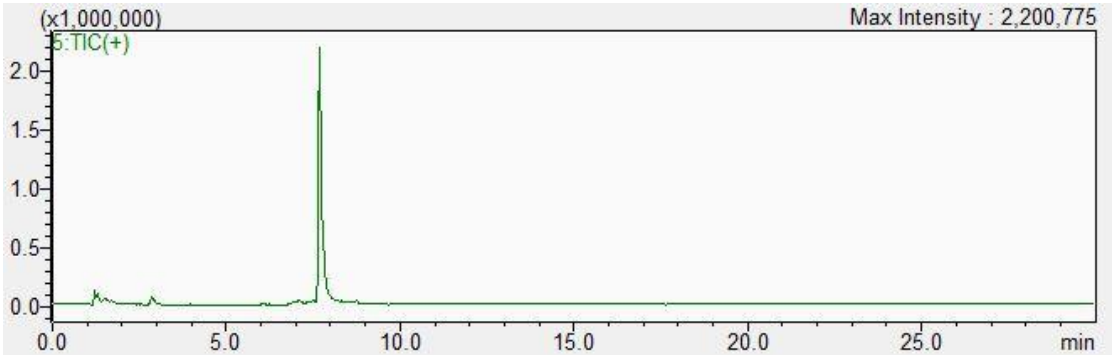

k) m/z = 341

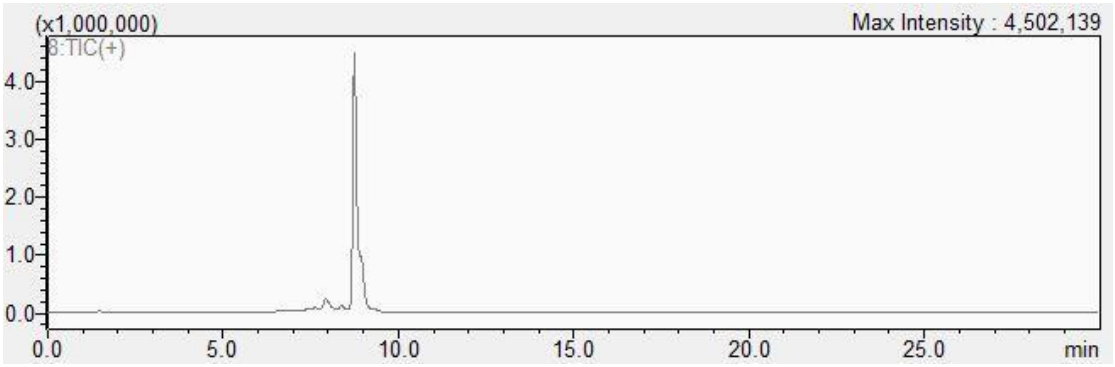

l) m/z = 343

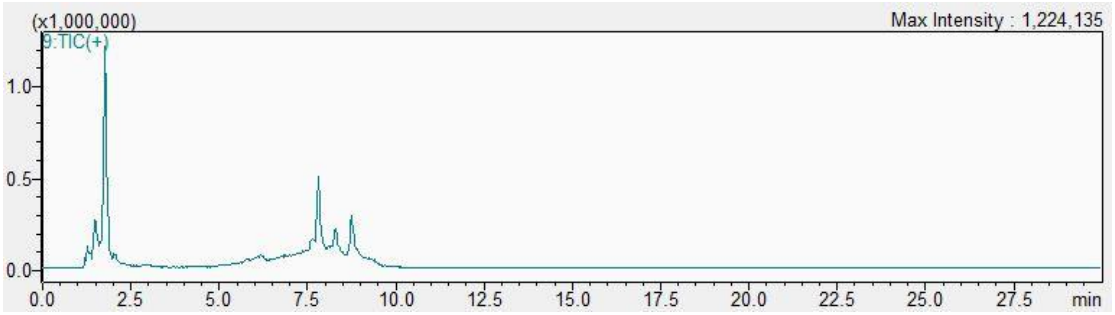

m) m/z = 391

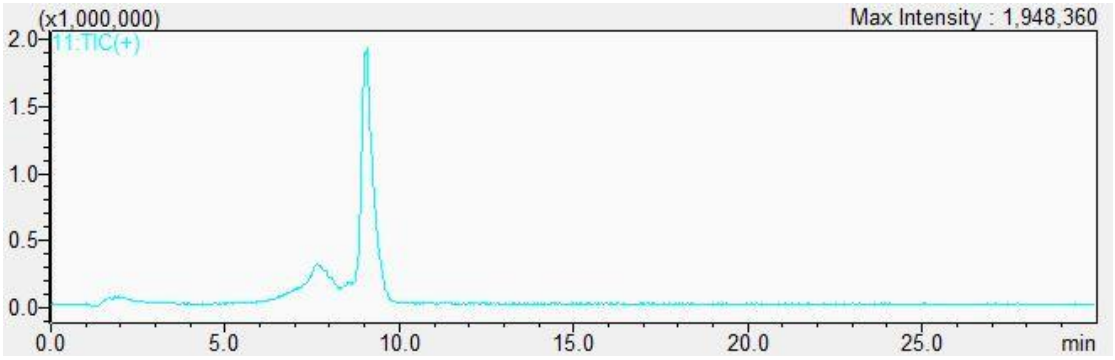

n) m/z = 413

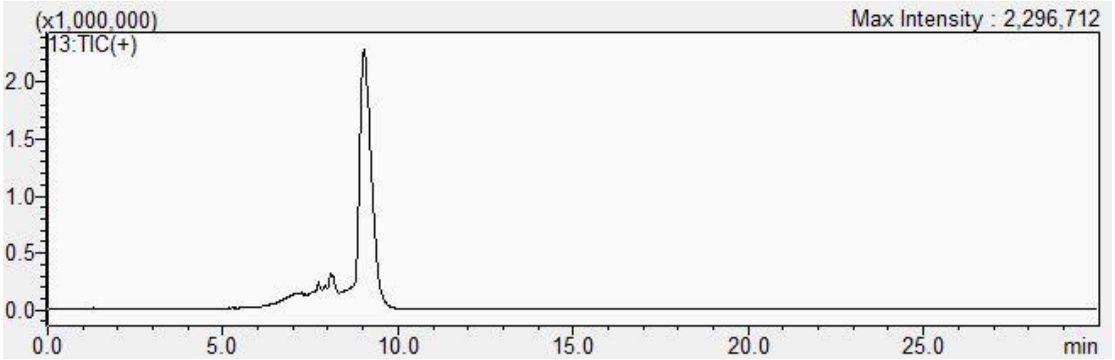

o) m/z = 445

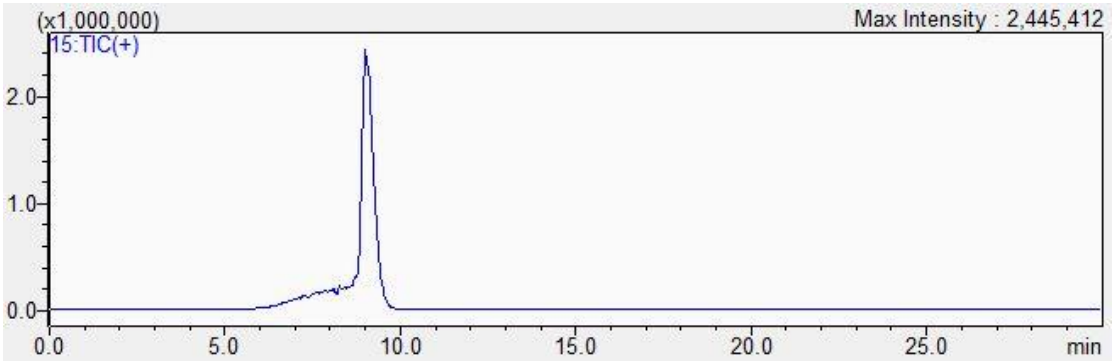

Figure 7-16: LC-MS/MS spectra of TMP degradation products a) 165, b) 179, c) 183, d) 271, e) 274, f) 291(TMP), g) 307, h) 309, i) 325, j) 327, k) 341, l) 343, m) 391, n) 413, o) 445. Condition: $[TMP]_0$ = 10 mg/L, $[chlorine]_0$ = 15 mg/L as Cl_2, UV fluence = 154 mJ/cm^2, wavelength =275 nm, pH 8.